Revisiting Empirical Solar Energetic Particle Scaling Relations

I. Solar flares

Athanasios Papaioannou[1], Konstantin Herbst[2], Tobias Ramm[3], Edward W. Cliver[4], David Lario[5], and Astrid M. Veronig[6]

[1] Institute for Astronomy, Astrophysics, Space Applications and Remote Sensing (IAASARS), National Observatory of Athens, I. Metaxa & Vas. Pavlou St., 15236 Penteli, Greece
e-mail: `atpapaio@astro.noa.gr`
[2] Institut für Experimentelle und Angewandte Physik, Christian-Albrechts-Universität zu Kiel, 24118 Kiel, Germany
[3] Institut für Theoretische Physik und Astrophysik, Christian-Albrechts-Universität zu Kiel, 24118 Kiel, Germany
[4] National Solar Observatory, 3665 Discovery Drive, Boulder, CO 80303, USA
[5] NASA, Goddard Space Flight Center, Heliophysics Science Division, Greenbelt, MD 20771, USA
[6] Institute of Physics & Kanzelhöhe Observatory for Solar and Environmental Research, University of Graz, A-8010 Graz, Austria

November 29, 2022

ABSTRACT

Aims. The possible influence of solar superflares on the near-Earth space radiation environment are assessed through the investigation of scaling laws between the peak proton flux and fluence of Solar Energetic Particle (SEP) events with the solar flare soft X-ray peak photon flux.
Methods. We compiled a catalog of 65 well-connected (W20-90) SEP events during the last three solar cycles covering a period of ~34 years (1984-2020) that were associated with flares of class ≥C6.0 and investigated the statistical relations between the recorded peak proton fluxes (I_P) and the fluences (F_P) at a set of integral energies from E >10; >30; >60; to >100 MeV versus the associated solar flare peak soft X-ray flux in the 1–8 Å band (F_{SXR}). Based on the inferred relations, we calculate the integrated energy dependence of the peak proton flux (I_P) and fluence (F_P) of the SEP events, assuming that they follow an inverse power-law with respect to energy. Finally, we make use of simple physical assumptions, combining our derived scaling laws, and estimate the upper limits for I_P and F_P focusing on the flare associated with the strongest GLE yet directly observed (GLE 05 on 23 February 1956), and that inferred for the cosmogenic radionuclide based SEP event of AD774/775.
Results. We show that I_P and F_P scale with the solar flare SXR flux as $\propto F_{SXR}^{5/6}$. For the AD774/775 event (with a re-scaled upper limit F_{SXR} = X600) these scaling laws yield values of F_P at E>200 MeV of ~10^{10} cm^{-2} and ~1.5×10^9 cm^{-2} at E>430 MeV that are consistent with values inferred from the measurements of ^{14}C and ^{10}Be.

Key words. solar–terrestrial relations – solar energetic particles (SEPs) – solar flares – solar activity

1. Introduction

The radiation environment in a planetary star system is driven by its host star (Lammer et al. 2003; Airapetian et al. 2020). In the case of the solar system, the Sun determines this radiation environment (Temmer 2021), since it is the source of solar energetic particles (SEPs) while also modulating the incoming galactic cosmic ray (GCR) flux. SEP protons are accelerated at both solar flares and coronal mass ejections (CMEs) (Cane et al. 2010; Papaioannou et al. 2016; Reames 2021). SEP events that are limited in duration, reach small peak intensities, and have narrow emission cones, are thought to be associated with solar flares and type III radio bursts (see, e.g., Reames 2021). On the other hand, high-energy SEP events that can last for several days, achieve significant peak fluxes, have a broad cone of emission, are thought to be associated with CMEs and type II radio bursts (e.g., Desai & Giacalone 2016). The fact that high-energy protons can be accelerated both during the impulsive phase of flares and at CME-driven shocks (see, e.g. Forrest et al. 1985; Chupp et al. 1987; Cane et al. 2010; Papaioannou et al. 2016) complicates the interpretation of the mechanisms responsible for the acceleration, injection, and propagation of SEPs in the interplane-

tary (IP) medium (Klein & Dalla 2017), although the preponderant evidence favors CME-driven shocks as the dominant source of high-energy protons in the most intense large SEP events (e.g. Desai & Giacalone 2016; Cliver et al. 2022).

Large SEP events measured near Earth have been recorded by spacecraft over the last 60 years (for an example of the last ~ three solar cycles see, e.g., Fig. 15 (A) in Papaioannou et al. (2016)). Singular intense events, particularly at low (<30 MeV) energies, termed "rogue" SEP events by Kallenrode & Cliver (2001) occurred on 14 July 1959 (Bazilevskaya et al. 2010), 4 August 1972 (Lario et al. 2013; Knipp et al. 2018), 19 October 1989 (Vainio 2003; Lario et al. 2013), and 14 July 2000 (Belov et al. 2001; Lario et al. 2013; Mishev & Usoskin 2016). Such events are associated with multiple CMEs and converging shocks. In particular, the most intense SEP event identified so far during the modern space era occurred on 4 August 1972 with a peak proton flux at E> 10 MeV reaching 6×10^4 pfu (Kurt et al. 2004). The omnidirectional integrated fluence of this compound event at an integral energy of E> 30 MeV was estimated to be 5×10^9 cm^{-2} (Smart et al. 2006) and subsequently 8.4×10^9 cm^{-2} (Jiggens et al. 2014). A fraction of these large, gen-

erally soft-spectrum (Cliver et al. 2020a), SEP events, as well as numerous other events with harder spectra, can reach such high energies that particles can interact with Earth's atmosphere, and the sub-products are recorded on the ground as significant enhancements above the background GCR flux by neutron monitors (NMs; Mavromichalaki et al. 2011). Such events are termed Ground Level Enhancements (GLEs), reaching very high energies ($\geq$ 1-2 GeV) and posing a serious threat for humans and infrastructure (Shea & Smart 2012). Since 1956 a total of 73 GLEs have been reported by the global NM network[1] (Poluianov et al. 2017; Anastasiadis et al. 2019; Papaioannou et al. 2022). Investigating historical records of solar and geospace observations, researchers attempted to quantify one of the most extreme events that has ever been released by our Sun, known as the Carrington event, that occurred on 1–2 September 1859 (Cliver & Dietrich 2013). These authors estimated an omnidirectional fluence for the integral energy of E> 30 MeV of $\sim 1.1 \times 10^{10}$ protons cm^{-2}, which exceeds the relevant estimates of fluence of the modern era "rogue" events by a factor of $\sim$1.4. The Carrington event and its corresponding particle fluence were seen as the worst-case estimate of radiation hazard in the near-Earth environment that the Sun is capable of producing (Miroshnichenko & Nymmik 2014). However, with the help of cosmogenic radionuclide records, it became clear that much more extreme events, e.g., the event around AD774/775 might have occurred on the Sun (Miyake et al. 2012; Usoskin et al. 2013)[2].

The soft X-ray (SXR) peak flux of solar flares – regularly monitored since the mid 1970s by the *Geostationary Operational Environmental Satellite Program (GOES)* in the 1-8 Å (long) passband – has been widely used by the scientific community. Flares that are associated with intense variations in the radiation environment are categorized into three X-ray flare classes, namely C-, M- and X-class flares[3]. The largest solar flare that has ever been observed on the Sun in the modern era of spacecraft measurements occurred on 4 November 2003 and resulted in the saturation of the GOES X-ray detector. Its magnitude was estimated by linear extrapolation to be $\sim$X35 (Kiplinger & Garcia 2004; Cliver & Dietrich 2013) and, more recently, X30 (Hudson et al. 2022 (in preparation)). Between 1976 and 2020, there have been 22 solar flares with a magnitude $\geq$ X10 (see Table 4 of Cliver et al. 2020b). Research focusing on the largest SXR flares on the Sun provides estimates that reach up to several times X100. For example, Tschernitz et al. (2018) indicated that for the largest active regions (ARs), flares with $\sim$X500 magnitude could be produced. Recently, from consideration of various "worst case" estimates of the most intense solar flare based on the largest spot group observed in the last $\sim$150 years (6132 millionths of a solar hemisphere on 8 April, 1947, Cliver et al. (2022)) obtained a consensus value of $\sim$X200 (with bolometric energy $\sim 1.5 \times 10^{33}$ erg).

Several statistical studies point to an empirical relation between the SXR flare peak flux and the achieved peak proton flux and fluence of the resulting SEP events (see, e.g. Kahler 1982, 2001; Belov et al. 2005b; Cane et al. 2010; Papaioannou et al. 2016). Recent studies that investigated such correlations for a set of integral proton energies showed that the correlation of the SEP peak proton flux or the SEP fluence with the flare SXR peak

flux was reasonably stable (correlation coefficient $\sim$ 0.43) for all such energies considered (see e.g. Dierckxsens et al. 2015; Papaioannou et al. 2016).

In this work, we analyze the statistical relations among the SEP peak proton fluxes and omnidirectional fluences of a well-defined catalog of (initially) 67 events measured at 1 AU by *GOES* between 1984 and 2017 for a set of integral energies spanning E> 10-; E> 30-; E> 60-, and E>100 MeV and the SXR peak fluxes of their parent solar events. Takahashi et al. (2016) deduced that the upper limit for the peak proton flux (I_P) of E>10 MeV is proportional to the SXR flux ($I_P \propto F_{SXR}^{5/6}$). Based upon this result and expanding their argumentation, we derive upper limits and scaling relations among the SEP peak flux (I_P) at each integral energy (from E>10 to E>100 MeV) and the SXR peak flux (F_{SXR}). We extend these relations to incorporate also the fluence of the SEP events (F_P). We further calculate the integral SEP peak flux and fluence spectra, for the events in our sample, which are assumed to follow an inverse power law. We compare our findings with the most extreme peak proton fluxes and fluences that have ever been recorded for a GLE in modern times (Koldobskiy et al. 2021), viz., the strong hard-spectrum GLE that occurred on 23 February 1956 (GLE05), as well as with the superflare of AD774/775.

Based on estimates of the largest possible SXR flare, the obtained scaling laws, and the observations used in this work, we estimate the most intense SEP proton fluxes and fluences that the Sun can produce, as well as the corresponding SEP spectra (for both quantities). In the concluding section of this study implications for the effects of solar superflares on the radiation environment are put forward and discussed.

2. Data sets

SEP data were scanned from 1984 to 2020, aiming at identifying well-connected SEP events (W20-90°) that reached integral energies of E>100 MeV. No such events occurred between 2018 and 2020. We identified 67 well-connected SEP events between 1984 and 2017 that extended from E> 10 MeV to E> 100 MeV. However, two of these events had to be excluded from our analysis. This is because, our event selection is based on that of Herbst et al. (2019) who considered SEP events whose origin is temporary related to X-ray solar flares of class $\geq$C6.0. The solar flare characteristics of the remaining 65 events were obtained from the online repository of the National Oceanic and Atmospheric Administration (NOAA) [4]. Note that in order to get the accurate SXR fluxes, proper scaling has been applied (using a multiplicative factor of 1/0.7 for the GOES 1–8 Å channel)[5]; the saturated strong X-class event values also need further attention: their re-scaled SXR classes are taken from Hudson et al. (2022; in preparation).

For the SEP events between 1986 and 2017 we used the corrected[6] *GOES*/EPS data obtained from `https://satdat.ngdc.noaa.gov/sem/goes/data/avg/`. For each of the identified SEP events we have been able to identify the peak intensity (in units of protons cm^{-2} sr^{-1} s^{-1}, 5-min averages) in their prompt component, similar to Lario & Karelitz (2014), which is understood as the maximum intensity observed shortly after the

---

[1] `https://gle.oulu.fi/`
[2] At present, analyses of ice cores for the ^{36}Cl cosmogenic nuclide have revealed no evidence for a significant low-energy SEP event in 1859 (Cliver et al. 2022)
[3] with their range varying between $10^{-6} - 10^{-5}, 10^{-5} - 10^{-4}$ & above 10^{-4} W/m^2, for the C-, M- and X-classes, respectively

[4] `https://www.ngdc.noaa.gov/stp/space-weather/solar-data/solar-features/solar-flares/x-rays/goes/`
[5] `https://www.ngdc.noaa.gov/stp/satellite/goes/doc/GOES_XRS_readme.pdf`
[6] `https://ngdc.noaa.gov/stp/satellite/goes/datanotes.html`

onset of the event in-situ and several hours or days before the particle enhancement commonly associated with the arrival of an interplanetary shock (if any) at the spacecraft (i.e., energetic storm particles or the ESP component were excluded). For some events, the maximum intensity in the prompt component is observed as a plateau in the time-intensity profile before the local enhancement associated with the passage of shocks (Reames & Ng 1998). In these cases, the peak intensity is taken as the maximum value of the intensity plateau. One should further note that different *GOES* satellites may record different time profile because of their positions in space and calibration dissimilarities. In this work, we scanned through all the available recordings and spacecraft, selecting those *GOES* satellites that had the highest peak flux. Moreover, from the retrieved integral proton intensities, we have computed the omni-directional time-integrated fluences (in units of protons cm^{-2}) by integrating each channel throughout the SEP event and multiplying the result by 4π (Lario & Decker 2011). Since the repository mentioned above provides no integral data for three SEP events marked earlier, i.e., in 1984-1985, we used the peak proton flux and fluence values that are included in the paper by Papaioannou et al. (2016). The obtained *GOES* peak proton fluxes, fluences, and the particular GOES satellite used for each SEP event are tabulated in Appendix C.

3. Scaling relations

3.1. SXR flare flux and peak proton fluxes

As a first step, we obtain the scaling relations between the SXR magnitude of the solar flares (F_{SXR}) and the peak proton flux (I_P) for the integral energies E> 10 MeV, E> 30 MeV, E> 60 MeV, and E> 100 MeV. The proportionality relationships between F_{SXR} and I_P have been primarily investigated for an integral energy of E> 10 MeV (see Belov et al. 2007; Cliver et al. 2012; Herbst et al. 2019). However, our goal is to further investigate these relations up to higher energies, quantify whether they vary, and thus identify and quantify the conditions that lead to a potential variability.

Figure 1 shows a scatter plot of the E>10 MeV peak proton flux vs. the X-ray flare intensity for the 65 SEP events in our sample (blue dots). The solid black line is the best-fit regression to the data in the log-log space. Similar to Cliver et al. (2012); Cliver & Dietrich (2013), and Herbst et al. (2019) here we use the Reduced Major Axis (RMA) method, while most commonly, the ordinary least-square (OLS) regression is employed (e.g. Belov et al. 2005b). However, the RMA is specifically formulated to handle errors in both variables at use (Harper 2014) and a non-causal relationship between the two variables is assumed (see details in Till 1973). As a result, $I_P \propto F_{SXR}^{\beta}$ with β=1.40±0.19 was retrieved. Additionally, the gray shaded envelope in Fig. 1 provides an error estimated while employing the fitting routine provided at `https://docs.scipy.org/doc/scipy-0.19.0/reference/generated/scipy.optimize.leastsq.html`. In detail, the Jacobian matrix is multiplied with the residual variances, estimated by the mean square errors. The resulting covariance matrix then is used to derive the standard error and, therefore, the ±σ uncertainty obtained from the fit (correlation coefficient is cc=0.46). Based on Takahashi et al. (2016) the upper limit of the I_P - F_{SXR} relation is given by $I_P \propto F_{SXR}^{5/6}$ (dashed red line). This relationship is based on a chain of assumptions that brings together solar flares, CMEs, and SEPs. The starting point of this relation is the SXR flux (F_{SXR}), which
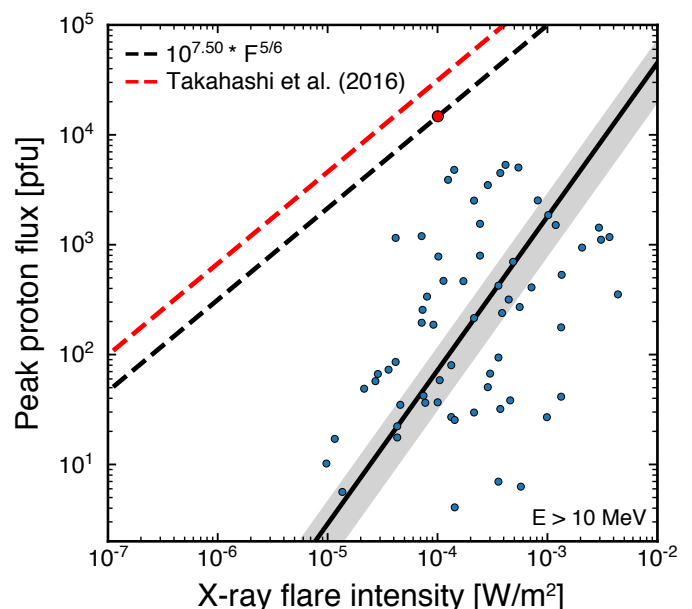

Fig. 1. Scatter plot of the E>10 MeV peak proton flux vs. the X-ray flare intensity of our new sample (blue dots). The solid black line corresponds to the RMA regression fit of our sample corresponding to $I_P \propto F_{SXR}^{\beta}$ with β=1.40±0.19. The red dashed line gives the upper solar limit from Takahashi et al. (2016) based on a scaling law of $I_P \propto F_{SXR}^{5/6}$. In the figure, this relation was re-scaled to the upper-point in our sample presented as a red dot, suggesting a new upper limit that is slightly below the previously reported limit by Takahashi et al. (2016).

is the most commonly used index of flare magnitude. Takahashi et al. (2016) assumed that F_{SXR} is roughly proportional to the total energy released during flares (E_{flare}) i.e., $F_{SXR} \propto E_{flare}$. In addition, they argued that the kinetic energy of the CME (E_{CME}) is proportional to E_{flare} and that the CME mass (M_{CME}) is the sum of mass within the gravitationally stratified AR. Finally, these authors further assumed that the total kinetic energy of solar energetic protons is proportional to E_{flare} and that the duration of the proton flux enhancement is determined by the CME propagation timescale. As a result, the energetic proton flux I_P in response to the SXR flare class (F_{SXR}) is scaled as:

$$I_P \propto F_{SXR}^{5/6} \tag{1}$$

As can be seen, there is only one SEP event in our sample that had an I_P larger than 10^4 pfu (i.e., 8 November 2000). This event was associated with an M7.0 SXR flare and hence stands out in the plot as the central uppermost data value (we have indicated this event with a red filled circle in Fig. 1). This remarkable SEP event (see Cliver et al. 2019) was associated with a well-connected source (W77^o, e.g., Lario et al. 2003), a wide (>170°) and fast CME (~1700 km/s, see Thakur et al. 2016), a long-lasting type II radio burst (Agueda et al. 2012) and a complex type III radio emission (Cane et al. 2002). Although this SEP event had the potential to be registered by NMs and hence be listed as a GLE, there was no increase measured at ground-based detectors (Bütikofer et al. 2021). For this event, the height where the CME-driven shock formed, based on type II radio burst measurements, was estimated to be ~ 3.5 $R_{\odot}$ (Thakur et al. 2016). This height is a factor of ~2.3 above the median CME height for GLEs and probably too high to accelerate GLE particles. We used the same theoretical arguments that were put forth by Takahashi et al. (2016) and thus the slope of the upper limit is kept
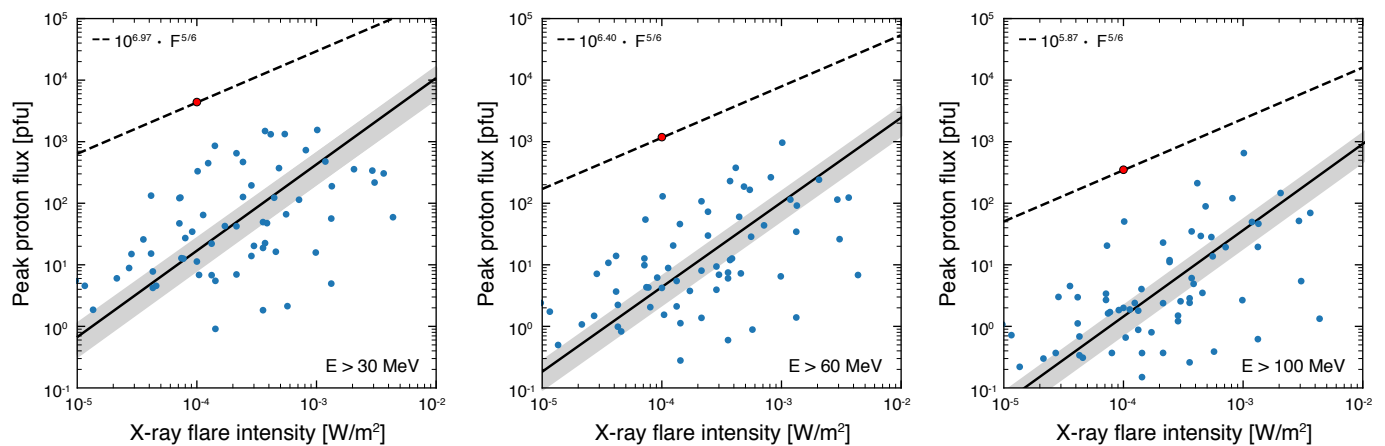
Fig. 2. Similar to Fig. 1. From left to right, these panels present results for E>30-; E>60-; and E>100 MeV, respectively. The solid black line corresponds to the RMA regression in each case. The black dashed line gives the upper solar limit based on the Takahashi et al. (2016) scaling law of $I_P \propto F_{SXR}^{5/6}$. The line is forced to fit the uppermost point in each panel. In all panels, the red dot correspond to the 8 November 2000 outstanding large SEP event (see text for further details).

identical. However, based on our sample, this upper limit had to be re-scaled, as indicated by the dashed black line. It should further be noted that the Takahashi et al. (2016) sample is inclusive of the uppermost point in our sample (i.e. 8 November 2000). Their sample includes an even stronger event (on 4 November 2001) with a larger peak proton flux of 31700 pfu associated with an X1.0 SXR flare[7]. As we have done in Figure 1, Takahashi et al. (2016) scale the theoretically derived $\propto F_{SXR}^{5/6}$ law in order to go through this extreme point. The 4 November 2001 event was not considered in our sample since: (a) the associated flare was located at W18° and thus outside our W20°-W90° bin and (b) the obtained peak proton flux was related to the arrival of the CME-shock at Earth (Shen et al. 2008). Hence, the resulting equation of this line for our sample is a more realistic and yet conservative upper limit of $I_P = 10^{7.50} \cdot F_{SXR}^{5/6}$.

Table 1. Slopes of the $I_P - F_{SXR}$ relation and correlation coefficients (cc) for each integral energy, derived in this work.

Integral Energy [MeV]	Slope $I_P - F_{SXR}$ (β)	Correlation Coefficient (cc)
E > 10	1.40±0.19	0.39
E > 30	1.38±0.19	0.44
E > 60	1.38±0.17	0.49
E > 100	1.41±0.17	0.52

We then obtained similar solar scaling relations of the form $I_P \propto F_{SXR}^{\beta}$ for the integrated E>30 MeV, E> 60 MeV, and E> 100 MeV energy channels. Our results are presented in Fig. 2, where the I_P-F_{SXR} relations similar to Fig. 1 for E>30 MeV (left panel), E> 60 MeV (middle panel), and E> 100 MeV (right panel) are displayed. Table 1 summarizes the slopes obtained by the RMA regression fits of each of the individual cases.

The exponent (power-law index) β seems to be relatively constant (~1.40) among the different energies, implying energy-independent slopes due, at least in part, to the inter-relatedness of the four integral energies considered. The correlation coefficients of the $I_P - F_{SXR}$ relation seem to increase with energy. A

somewhat similar trend has also been reported by Dierckxsens et al. (2015).

3.2. From peak fluxes to fluences

As described in Section 2, the peak proton flux per integral energy and the fluence were calculated for each of the 65 SEP events under study (see Appendix C). In the next step, scaling relations between fluences (F_P) and I_P are derived. Although the scientific community routinely uses I_P values to associate SEP events to their parent solar events (Cane et al. 2010; Papaioannou et al. 2016; Desai & Giacalone 2016), the time-intensity profiles [$I_{(t)}$], resulting from the convolution of SEP acceleration and transport processes, are also needed. This is especially important when quantifying the radiation environment. Following the procedure discussed in Kahler & Ling (2018) we compared the measured fluences (F_P) and peak proton fluxes (I_P) for each integral energy investigated in this study. In agreement with Kahler & Ling (2018), robust correlations ($cc \approx 0.97$) between F_P and I_P for each integral energy are found with slopes near unity. Thus, our results indicate energy-independence in the relationship between I_P and F_P. The details of these relations and the corresponding validation and verification comparisons are discussed in Appendix A.

Once the fluences (F_P) are derived from the data, we obtained the corresponding relations between $F_P \propto F_{SXR}$ by employing the RMA regression method (similar to the relations discussed in Section 3.1). The derived slopes $F_P - F_{SXR}$ and correlation coefficients are presented in Table 2. The correlation coefficients show a relative increase with respect to the increasing integral energy, starting at 0.43 for E>10 MeV and reaching 0.54 for E>100 MeV.

3.3. Integral energy spectra for the sample events

For each of the 65 SEP events in our sample, we fit the derived peak fluxes and fluences at the four integral energies under consideration with an inverse power-law ($A^{-\epsilon}$). We then compute a mean and median spectrum (i.e., I_P vs > E and F_P vs > E) as follows: (a) Determine the sample mean and median values of I_P and F_P at each of the four energies based on the fitted values of

---

[7] see http://cdaw.gsfc.nasa.gov/CME_list/sepe/

Table 2. Slopes of F_P-F_{SXR} and correlation coefficients (*cc*) for each integral energy, derived in this work.

Integral Energy [MeV]	Slope $F_P - F_{SXR}$ (δ)	Correlation Coefficient (cc)
E > 10	1.59±0.21	0.43
E > 30	1.56±0.20	0.48
E > 60	1.48±0.18	0.52
E > 100	1.44±0.17	0.54
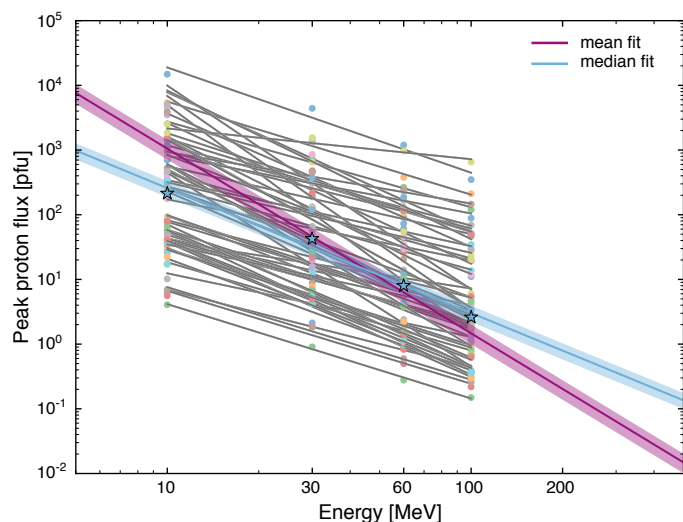
Fig. 3. The derived spectrum for each of the 65 SEP events, assumed to follow an inverse power-law, is presented as a solid gray line. The mean spectrum is shown as a continuous magenta line (ϵ_{mean} = 2.87), while the blue line provides the median spectrum (ϵ_{median}= 1.96). Blue star symbols depict the median peak proton flux values per energy.

these parameters for the 65 events; (b) Fit these values under the same assumption of inverse power-law dependence.

The results for the integral spectra of peak proton fluxes are presented in Fig. 3. Here, the colored dots represent the measured I_P values of each SEP event, while the solid gray lines show the event-dependent inverse power-law fits. In addition, the solid purple and blue lines represent the mean (ϵ_{mean}=2.87) and median (ϵ_{median}=1.96) spectra derived from our SEP sample, respectively.

4. Estimating the peak proton flux and fluence for solar superflares

4.1. Estimates and arguments

In this section, we attempt to estimate the uppermost peak proton fluxes (I_P), and fluences (F_P) for two notable SEP parent flares. Namely, we focus on the event of 23 February 1956 (GLE05) (Belov et al. 2005), the most intense high-energy SEP event of the modern era, and the AD774/775 SEP event (Cliver et al. 2020b). The radionuclide records show peak-like increases in the order of 12‰ around AD774/775. Since no information on the corresponding SEP spectrum is known for such an event, a scaling of GLE05 is usually assumed, with a multiplicative value of 70±30 applied to the 1956 SEP spectrum to obtain that of AD774/775 (see Table 1 of Usoskin et al. 2021).

The SEP-to-SXR flare scaling law of Takahashi et al. (2016) in Eq. (1) is shown as dashed black lines in Figs. 1 and 2. In each plot, the relations are positioned to run through the most intense

SEP events of our sample so that we can discuss the upper limits of the peak proton flux ($I_{P,upper}$) in response to F_{SXR}. Based on our sample

$$I_{P,upper} = I_{P,energy} \cdot F_{SXR}^{5/6}, \qquad (2)$$

with $I_{P,E10} = 10^{7.50}$ pfu, $I_{P,E30} = 10^{6.97}$ pfu, $I_{P,E60} = 10^{6.40}$ pfu, and $I_{P,E100} = 10^{5.87}$ pfu, and F_{SXR} is normalized in units of 1 W/m^2

Combining the peak proton flux and fluence relations from Appendix A (see Fig. A.1) with the fits from the dashed lines in Fig. 1 and 2, the upper-limit fluences $F_{P,upper}$ are found to be best described by:

$$F_{P,upper} = F_{P,energy} \cdot (F_{SXR}^{5/6})^\delta, \qquad (3)$$

where $F_{P,E10} = 10^{5.48} \cdot (10^{7.50})^\delta$ cm^{-2}, $F_{P,E30} = 10^{5.46} \cdot (10^{6.97})^\delta$ cm^{-2}, $F_{P,E60} = 10^{5.51} \cdot (10^{6.40})^\delta$ cm^{-2} and $F_{P,E100} = 10^{5.53} \cdot (10^{5.87})^\delta$ cm^{-2}, and F_{SXR} is normalized in units of 1 W/m^2. The values of δ can be found in Appendix A (see Table A.1). These results are used in Fig. 4 to show the $F_P - F_{SXR}$ *upper limit* relations for each integral energy, as an orange line.

The solid black lines shown in Fig. 4 correspond to the RMA regression applied to the 65 SEP events (see Table 2) embedded in the error band (gray shaded area), while the relationship in Eq. (3) is represented by orange lines, and the dashed black lines present an alternative upper limit based on the RMA fit shifted to fit the uppermost F_P values of the SEP sample.

4.2. Solar flares in February 1956 and AD774/775

The 23 February 1956 GLE event (GLE05) is the most extreme GLE event yet recorded, with a similar structure to the 20 January 2005 event (GLE69). The strongest solar flare in February 1956 occurred when the AR group 17351 was near the west limb as seen from Earth. At this time, a solar flare of Hα importance class 3B, located at N25 W85, was initiated at 03:34 UT and produced this notable GLE (Belov et al. 2005a). The fluence of GLE05 at an integral energy of E > 430 MeV (> 1 GV in rigidity) was calculated to be 4.21×10^7 cm^{-2} (Usoskin et al. 2020) being almost one order of magnitude higher than the fluence of any other known GLE (see Table 1 of Cliver et al. 2020b), making it the largest SEP event ever recorded by modern instrumentation.

By examination of concentrations of cosmogenic nuclides sequestered in tree rings and ice cores, intense SEP events have been identified in the distant past. The AD774/775 event was the first such event discovered as an exceptional increase in ^{14}C concentration (12‰) in tree rings (Miyake et al. 2012). This increase was investigated independently in detail by many different groups (e.g. Usoskin et al. 2013; Mekhaldi et al. 2015; Büntgen et al. 2018) verifying its solar origin (Mekhaldi et al. 2015). As a result, this exceptional SEP event was recently modeled by a SEP fluence spectrum ~ 62 times that of GLE05 (Cliver et al. 2020b, see their Table 1), thus obtained a E>430 MeV fluence of 2.6×10^9 cm^{-2} for the AD774/775 event, making it one of the most powerful inferred SEP events to date. This corresponds to the consensus value of several of these independent studies of ^{14}C and ^{10}Be concentrations in tree rings and ice cores. More such SEP superevents have been found in the cosmogenic radionuclide records: AD993/994 (Miyake et al. 2019), 660 BC
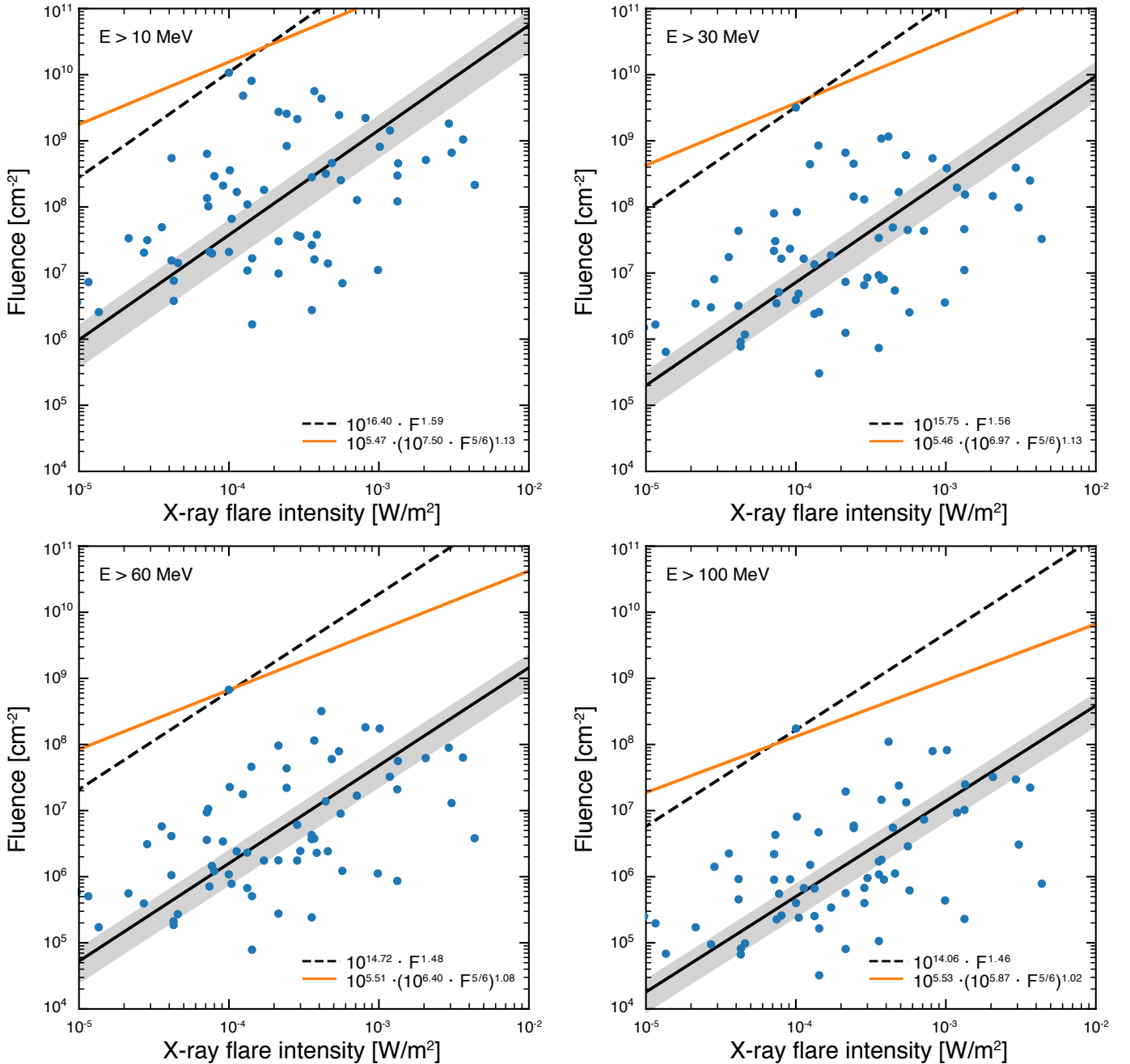
Fig. 4. $F_P \propto F_{SXR}$ relations for the four integral energy bands of the SEP events, i.e., E>10 (top left); E>30 (top right); E>60 (bottom left); and E>100 MeV (bottom right). The log-log relations are obtained with the RMA regression fitting (solid black line). The estimated upper limits of F_P in terms of F_{SXR} based on Takahashi et al. (2016) are depicted as solid orange lines in each panel. The dashed black line are lines similar to the RMA one scaled to the uppermost point of the sample.

(O'Hare et al. 2019), and most recently 5410 BC (Miyake et al. 2021), 7176 BC, 5259 BC (both discussed in Brehm et al. 2021), and 9125 BP (Paleari et al. 2022), but thus far no estimates of the corresponding SXR flare class has been made for these events.

Cliver et al. (2020b) estimated that F_{SXR} associated with the 23 February 1956 GLE event ranged from X10 to X30, and from this estimate obtained a SXR class of X145 to X425 for the AD774/775 flare. In particular, Cliver et al. (2020b); their Figure 7, applies an RMA fit to a scatter plot of modeled E>200 MeV fluences from Raukunen et al. (2018) for hard-spectrum GLEs vs. the peak intensities of their associated SXR flares. They then added two points for the 1956 GLE (i.e. GLE05) based on the

estimated range of the peak SXR intensity (X10-X30) of its associated flare (as inferred from white-light, radio, sudden ionospheric disturbances, comprehensive flare index, inferred CME transit time, and geomagnetic storm observations) and its E>200 MeV fluence (Usoskin et al. 2020). Through these points, they extrapolated lines parallel to the RMA fit to the modeled E>200 MeV fluence for the AD774 SEP event to obtain an estimate of X285±140 for the AD774 flare. Based on the NOAA reassessment of the recent SXR calibration, these values were corrected to X14 to X42 (GLE05) and X200 to X600 (AD774/775), respectively (see Cliver et al. 2022). Following Eq. (1) of Cliver
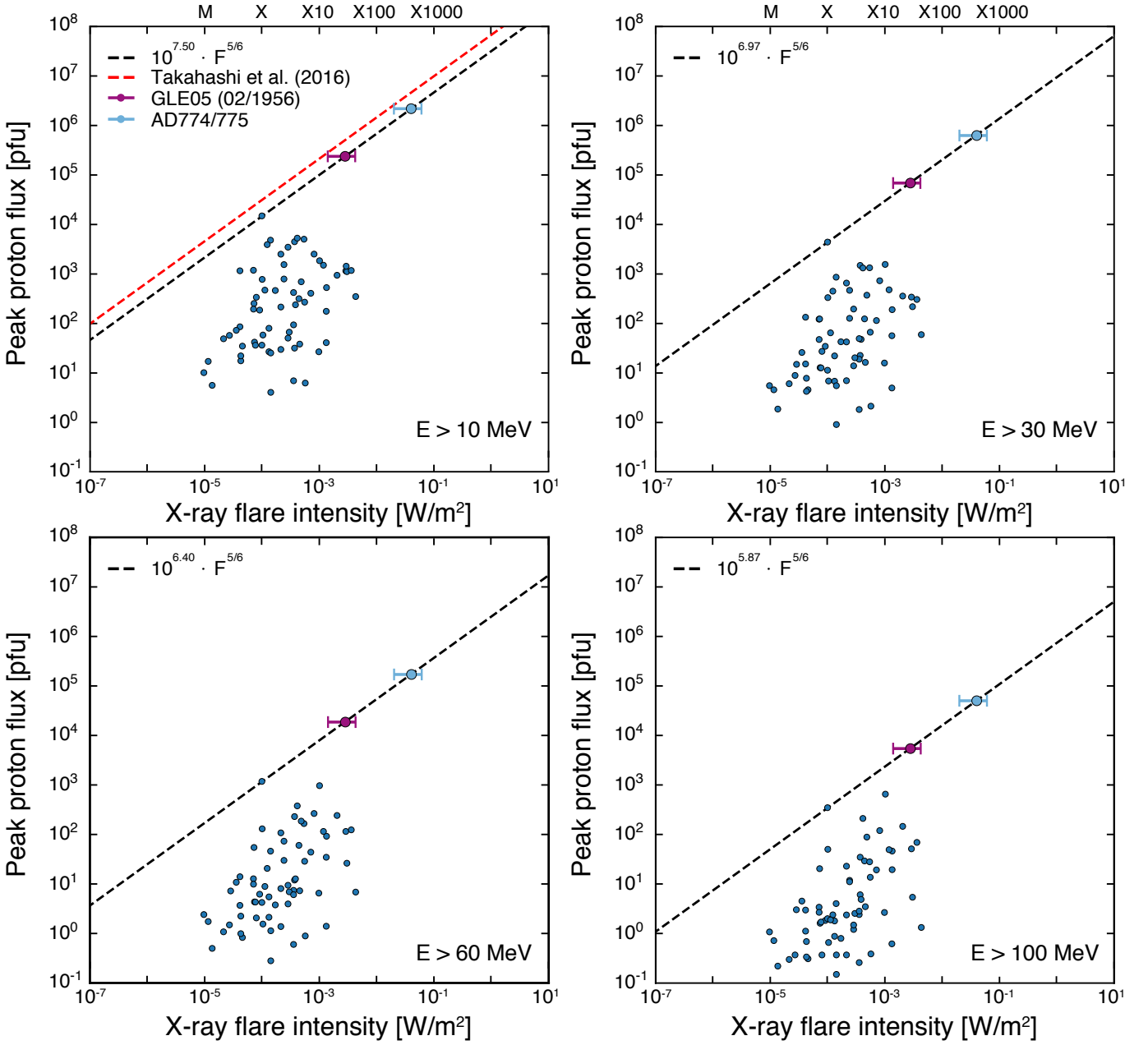
Fig. 5. $I_P \propto F_{SXR}$ relations for the four integral energy bands of the SEP events, i.e., E>10 (top left); E>30 (top right); E>60 (bottom left); and E>100 MeV (bottom right). The estimated upper limits for the events of 23 February 1956 and AD774/775 are represented as purple and cyan filled circles, respectively. The plotted SXR intensities were obtained by dividing the values in Appendix C by 0.7 to reflect the recent NOAA recalibration (Hudson et al. 2022 (in preparation); Cliver et al. 2022).

et al. (2020b), corrected for the SXR flux shift[8], the flare bolometric energy for the upper limits of the SXR associated flares for the nominal values of each of these SEP events currently is $\sim 3 \times 10^{32}$ erg (1956) and $\sim 2 \times 10^{33}$ erg (AD774/775), respectively. A value of 4×10^{32} is comparable to the 3.6×10^{32} value for 28 October 2003 and the 4.3×10^{32} value for the 4 November 2003 (from TIM measurements; Emslie et al. 2012). A flare with a bolometric energy of $\sim 2 \times 10^{33}$ erg satisfies the $> 10^{33}$ erg criterion (Schaefer et al. 2000) for a superflare.

4.3. SEP peak fluxes, (I_P) & fluences (F_P) driven by F_{SXR}

Figure 5 shows the $I_P - F_{SXR}$ relations for the four respective integral energy bands. The estimated upper limit of the peak proton fluxes of GLE05 and AD774/775 are indicated by the purple and blue filled circles, respectively. They are based on the mean SXR fluxes provided by Cliver et al. (2020b), adjusted upward by a factor of $1/0.7$;$\sim 40\%$ for the NOAA recalibration (Hudson et al. 2022; in preparation), and range from X28±14 (GLE05) and $\sim$X400±200 (AD774/775). Substituting the corresponding F_{SXR} in Eq. (2) then leads to the expected upper peak proton flux limits. The dashed black lines further present the upper limits given by Eq. (2), based on which the upper limit I_P for GLE05 (based on $F_{SXR} = $ X42) is $I_{P,E>10} = 3.31 \times 10^5$ pfu, $I_{P,E>30} = 9.76 \times 10^4$ pfu, $I_{P,E>60} = 2.63 \times 10^4$ pfu and $I_{P,E>100} = 7.75 \times 10^3$ pfu.
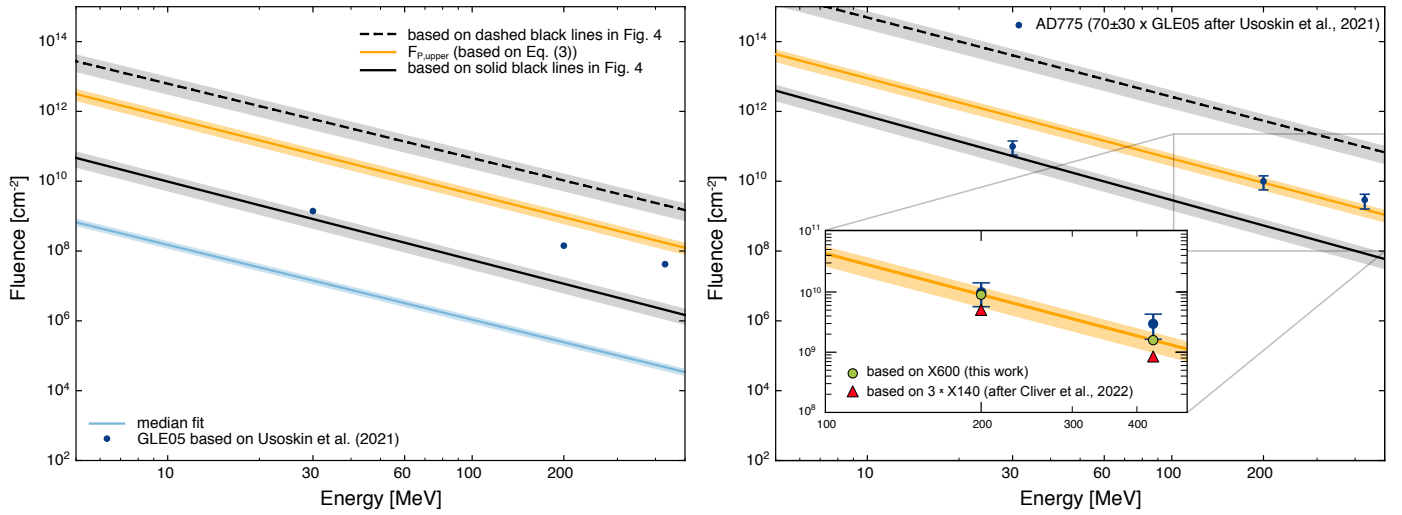
---

[8] $F_{TSI} = 0.33 \times 10^{32} (C_{GOES}/C_{GOES,X1.4})^{0.72}$, F_{TSI} is the Flare Total Solar Irradiance of bolometric energy and $C_{GOES}/C_{GOES,X1.4}$ equals the flare SXR class scaled to X1.4

Fig. 6. Derived fluence spectra for the two solar cases under investigation. The left panel corresponds to GLE05 while the right panel corresponds to the AD774/775 SEP event. These plots are similar to Fig. 3 but for a fluence with the addition of the relevant data points for each event (based on Usoskin et al. (2021)), depicted as filled blue circles and the corresponding derived spectra calculated for each case from the relations presented in Sec. 3. The median spectra is shown as a light blue line with the corresponding error depicted with a gray shade.The green filled circles in the inset represent the upper limit (i.e. based on an X600 SXR flare) obtained fluence for E>200 MeV and E>430 MeV derived by the orange line. The red triangles represent the same fluence values but for a 3 x ~X140 SXR flare (Cliver et al. 2022). See text for details.
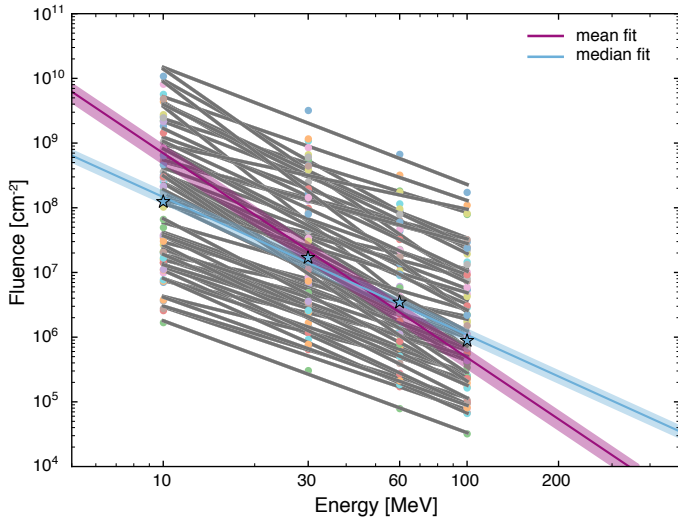

Fig. 7. This figure is similar to Fig. 3 but for fluence. The derived fluence spectrum for each of the 65 SEP events is presented as a solid black line, per event. The mean spectrum is shown as a continuous magenta line (ϵ_{mean}=3.16), while the blue line provides the median spectrum (ϵ_{median}=2.13). Blue star symbols depict the median fluence values per energy.

Table 3. *Upper limit* Peak Proton Fluxes (I_P, [pfu]) and Fluences (F_P, [cm^{-2}]) for the SEP event on AD774/775 and GLE05 derived in this work, for each integral proton energy. Peak proton fluxes were calculated via Eq. 2 and Fluence via Eq. 3 for a given SXR flux. The upper and lower limits included in the Table are driven by the F_{SXR} range of the associated solar flare per event, taken from Cliver et al. (2022).

	AD774/775	GLE05
Integral Energy	**Peak Proton Flux – I_P**	
(MeV)	**(pfu)**	**(pfu)**
E > 10	2.16E+06$^{3.03E+06}_{1.21E+06}$	2.36E+05$^{3.31E+05}_{1.32E+05}$
E > 30	6.38E+05$^{8.95E+05}_{3.58E+05}$	6.96E+04$^{9.76E+04}_{3.91E+04}$
E > 60	1.72E+05$^{2.41E+05}_{9.64E+04}$	1.87E+04$^{2.63E+04}_{1.05E+04}$
E > 100	5.07E+04$^{7.11E+04}_{2.85E+04}$	5.53E+03$^{7.75E+03}_{3.10E+03}$
Integral Energy	**Fluence – F_P**	
(MeV)	**(cm^{-2})**	**(cm^{-2})**
E > 10	4.25E+12$^{6.23E+12}_{2.21E+12}$	3.48E+11$^{5.09E+11}_{1.81E+11}$
E > 30	1.05E+12$^{1.53E+12}_{5.45E+11}$	8.56E+10$^{1.25E+11}_{4.45E+10}$
E > 60	1.46E+11$^{2.10E+11}_{7.82E+10}$	1.33E+10$^{1.92E+10}_{7.14E+09}$
E > 100	2.13E+10$^{3.01E+10}_{1.18E+10}$	2.23E+09$^{3.14E+09}_{1.24E+09}$

For the AD 774/775 event (based on F_{SXR}=X600) this would be: $I_{P,E>10} = 3.03 \times 10^6$ pfu, $I_{P,E>30} = 8.95 \times 10^5$ pfu, $I_{P,E>60} = 2.41 \times 10^5$ pfu and $I_{P,E>100} = 7.11 \times 10^4$ pfu (see also Table 3).

Following the same reasoning, the upper limit fluences (F_P) in terms of F_{SXR} for each event were then calculated utilizing Eq. (3), with the relevant $F_{P,energy}$ per case. These upper limits are given as orange lines in each of the panels of Fig. 4. A summary of the results for both the upper limit peak proton flux and fluence at each integral energy of interest for GLE05 and the AD774/775 event are presented in Table 3.

4.4. Spectrum based on F_{SXR}

The dark blue circle points in Figure 6 give the fluence spectra for the February 1956 (left panel) and AD774/775 (right panel) SEP events. The blue circles in the left panel are estimates of the fluence of GLE05 given by Usoskin et al. (2020), while those for the AD774/775 event shown in the right panel are scaled by a factor of 70±30 (Usoskin et al. 2020, indicated by the error bars). Both panels in Figure 6 contain four lines (three of which are derived from similarly formatted lines [viz., black-dashed, orange, black-solid]) in Figure 4, and a fourth (light blue) line

directly taken from Figure 7. The three lines in Figure 6 that stem from Figure 4 are all constructed in the same way: fluences are obtained from the corresponding lines in each of the four energy panels in Figure 4 for a SXR class of X42 (1956) and ~X600 (AD774/775) for the left and right panels, respectively, in Figure 6. For each line, the shaded areas provide the error. The green filled circles in the inset of the right panel represent the calculated upper limit (i.e. based on an X600 SXR flare) fluence values for E>200 MeV and E>430 MeV directly derived from the orange line. Additionally, assessing the possibility of the corroboration of three closely timed, equal-fluence events in the case of AD774/775 an estimation of the resulting fluence based on a 3 x ~X140 flare was used (see details in Cliver et al. 2022). The red triangles in the inset of Fig. 6 show the obtained fluence for E>200 and E>430 MeV. The corresponding fluence is in reasonable agreement with that obtained in the case of a single eruptive flare source for the AD774 SEP event. In turn, this means that indeed episodes of multiple events could have taken place.

The obtained integral fluence spectra depicted by the dashed-black, solid-black, and solid-orange lines, respectively, in Fig. 6 are driven by the associated F_{SXR}, in this case an ~X600 class flare, corresponding to the upper limit range of the AD774/775 superflare, based on a 62 times multiple of the 1956 SEP spectrum (Cliver et al. 2020b). The plotted dark blue points for the slightly higher multiple of 70 from Usoskin et al. (2020) used to scale the AD774/775 SEP event to the 1956 GLE fall below (or within the uncertainty at E>430 MeV) the orange upper limit line based on the Takahashi et al. (2016) scaling relationship ($F_P - F_{SXR}^{5/6}$) in Figure 6. The proximity of the E>200 MeV and E>430 MeV points to the orange constraint line suggests that the AD774/775 event is close to the limit of what the Sun is capable of producing, for such an F_{SXR}, as has been surmised by others (see Figure 7.3 in Miyake et al. 2019).

4.5. Consideration of additional scaling relationships

In this section we consider two additional scaling laws, both prompted by a suggestion from our referee who proposed that: (a) we take into account a longer acceleration process within the inner heliosphere and assume that the peak proton flux (I_P) is proportional to $E_{flare} \cdot V_{CME}$. Combining $E_{flare} \propto F_{SXR}$ with $V_{CME} \propto F_{SXR}^{1/6}$ (see Takahashi et al. 2016) a scaling law of the form $F_{SXR}^{7/6}$ is derived (vs. the $F_{SXR}^{5/6}$ in Eq. (1); (b) we consider an "intermediate" scaling law in which direct proportionality of the peak proton flux (I_P) to the total number of accelerated particles at the energy under consideration is assumed and thus: $I_P \propto E_{flare} \propto F_{SXR}$. A scaling law of F_{SXR} practically leads to no difference at all for each of the integral energies employed in this work. On the other hand a scaling of $F_{SXR}^{7/6}$ leads to larger peak proton fluxes for stronger solar flares (i.e. larger F_{SXR}).

Figure 8 shows the evaluation of the scaling relation with F_{SXR} (panels on the left) and $F_{SXR}^{7/6}$ (panels on the right) against the scaling with $F_{SXR}^{5/6}$ in the case of the obtained fluences for the two events under consideration. Namely, GLE05 (top panels) and AD774/775 (bottom panels). As a result, for the first comparison (i.e. $F_{SXR}^{5/6}$ vs F_{SXR}) it seems that there is a marginal difference and in particular, we calculated that there is a mean relative factor, covering a wide energy range from E>10 to E>500 MeV, of 1.35 (2.13) for the case of GLE05 (AD774/775). For the second comparison (i.e. $F_{SXR}^{5/6}$ vs $F_{SXR}^{7/6}$) it seems that there is a difference of a factor of ~12 for lower energies (i.e. E>10

MeV) but the higher the energy the better the agreement between the scalings. Following the same procedure as before, the calculated mean relative factor for the same wide energy is 10.5 (6.64), for GLE05(AD774/775), respectively. More important is that all three possible scaling laws that are based on theoretical arguments, downstream of the Takahashi et al. (2016), offer a range of the obtained fluence for high energy particles (i.e. E>200 MeV) that are in agreement with each other within a factor of ~3.

5. Discussion & Conclusions

In this work, scaling relations of the peak proton flux (I_P) and the fluence (F_P) of large well connected SEP events recorded at Earth between 1984 and 2017, to the SXR peak fluxes (F_{SXR}) of their associated flares were investigated. In contrast to previous studies (e.g., Takahashi et al. 2016), the scaling relations discussed in this work (i.e., I_P or F_P vs F_{SXR}) are not limited to the integral proton energy of E>10 MeV but have also been calculated for a broader set of integral energies: E>30; E>60; and E>100 MeV.

In the case of the $I_P \propto F_{SXR}^{\beta}$ relations, we found that the power-law index β seems to be almost constant (~1.40) with increasing energy. This is consistent with the result of Belov et al. (2007) who used a different sample and employed the OLS method (instead of the RMA used in this work) and found that the slope for the $I_P \propto F_{SXR}$ relation is practically constant for E>10 MeV and E>100 MeV (~ 0.95). The results argue in favor of a relation between X-ray and proton emissions within uncertainties, without excluding other eruptive manifestations as, e.g., coronal mass ejections - CMEs. In particular, Takahashi et al. (2016) invoked proportional scaling laws among total flare energy (E_{flare}), CME kinetic energy, and the total SEP energy (E_{SEP}) to further derive a scaling of $I_P \propto V_{CME}^5$, assuming that the SEP event duration is inversely proportional to V_{CME}. Finally, calculations of the omnidirectional F_P values allowed for an investigation of the relations between I_P and F_P (see Appendix A for details).

The *upper limits* of I_P and F_P were explored with the application of the $F_{SXR}^{5/6}$ scaling relations (Eq. (2)) for I_P, as proposed by Takahashi et al. (2016) for the case of E>10 MeV, alone. In this work, we showed that the $I_P \propto F_{SXR}^{5/6}$ scaling relations could further be successfully translated to fluence (F_P) scaling relations (i.e., Eq. (3)). Furthermore, the obtained fluences and integral spectra seem to represent quite reasonably the fluences derived independently by other studies i.e., Usoskin et al. (2020), of the AD774/775 event within the uncertainty limits (orange line and green filled circles in Fig. 6). Moreover, we obtained similar results for two alternative scaling factors as shown in Figure 8.

Furthermore, the possibility that the AD774 SEP event was the result of multiple (i.e. two or three-equal fluence) events was assessed and it was shown that the corresponding SXR intensities fall well within that of the upper limit intensity for the case of a single eruptive flare source (see Fig. 6).

The scaling relations presented in this study provide a direct estimation of the upper limit peak proton flux (I_P), fluence (F_P), and spectrum ($\propto F_{SXR}^{5/6}$) based on the F_{SXR} flux of the driving solar flare. Therefore, the relations allow quantifying the effect of such a flare on the radiation environment, within uncertainties, caveats and assumptions. For instance, such scaling laws are inherently based on the assumption that the SEP events result from a scaling of the flare energy producing the SXR flares (e.g. Emslie et al. 2012). This is underlined by several studies, across
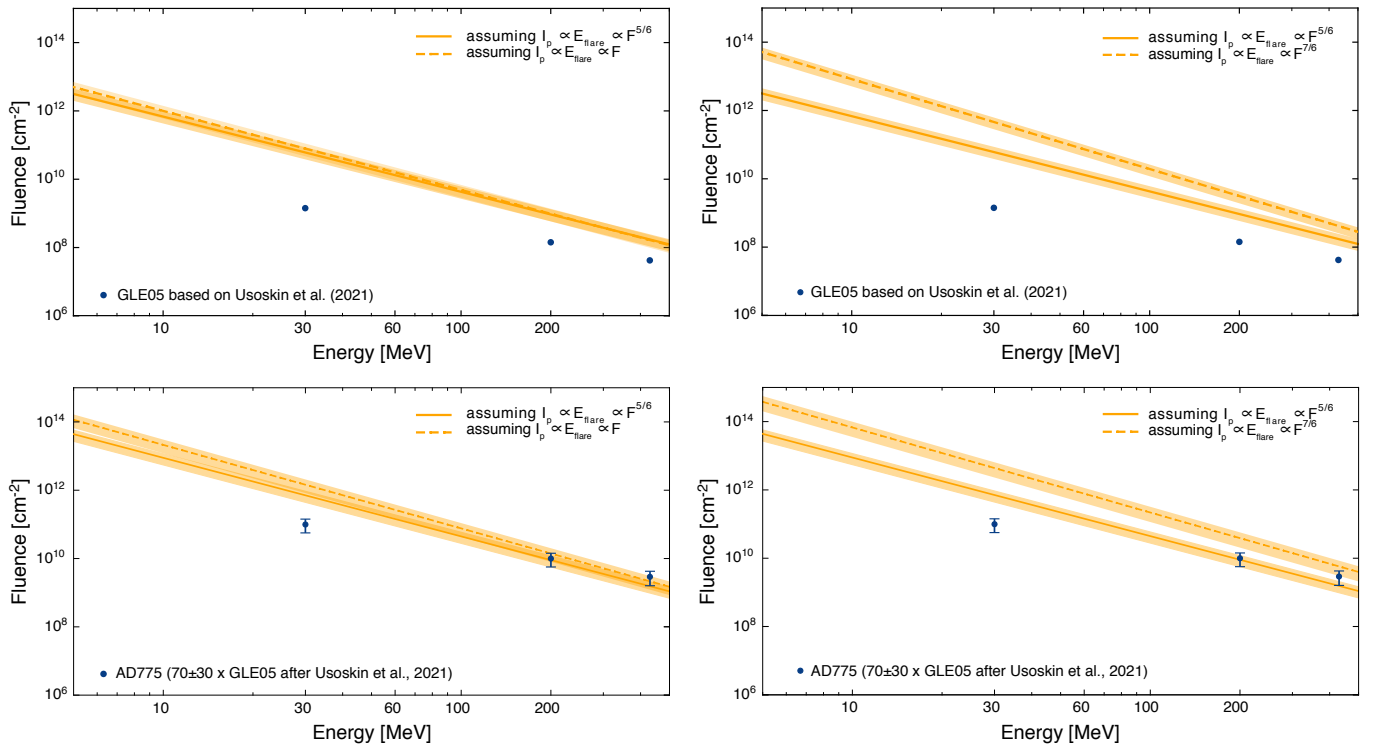
Fig. 8. Same as in Fig. 6 investigating the use of different scaling applications. Left panels: $I_P \propto E_{flare} \propto F_{SXR}^{5/6}$ (solid lines) vs. $I_P \propto E_{flare} \propto F_{SXR}$ (dashed lines). Right panels: $I_P \propto E_{flare} \propto F_{SXR}^{5/6}$ (solid lines) vs. $I_P \propto E_{flare} \propto F_{SXR}^{7/6}$ (dashed lines). The results for GLE05 are shown in the upper panels, those for AD774/775 in lower panels, respectively.

decades of research (e.g. Hudson 1978; Belov et al. 2005a; Belov et al. 2007; Cliver et al. 2012; Herbst et al. 2019) and suggest a casual relation between the solar eruption and the SEP production. Nonetheless, a recent detail work argues against a close physical relation of solar flares and SEPs (Kahler 2013) ignoring the evidence that flares associated with SEPs fundamentally differ from ordinary flares (Belov et al. 2007). Thus,our work begins with a sample of SEP events addressing the valid concern risen by Kahler (2013) that large SEP events do not arise in confined flares, making any general correlation between all flares and such SEP events problematic. CMEs can not be excluded from such an approach of scaling relations. In fact, the work of Cliver et al. (2012) showed that scaling relations of SEPs do take into account CMEs. This is because flares associated with fast CMEs ($V_{CME} > 1000km/s$) lead to similar scaling laws as those obtained for flares associated with SEPs. In addition, the correlation of fast CMEs to gradual SEPs have long been known (e.g. Kahler 2001, and references therein) while the works of Belov (2017), and Takahashi et al. (2016) further quantifies this. Recently Kahler & Ling (2020) showed that flares with no CMEs are quite similar to flares associated with slow CMEs, in contrast to those flares associated with fast CMEs; suggesting the possibility of two classes of flares. Such issues are noted here, and we should note that the scaling behavior of I_P to V_{CME} will be addressed in the second part of our study (i.e. *Part II*).

Another issue to take into account is the dependence of the obtained upper limit presented in this work on the 8 November 2000 SEP event. Thus, we further assessed the possibility to exclude this event and re-applied our proposed methodology. We found a difference of one-order of magnitude between the upper-limit spectra (inclusive of the 8 November 2000 SEP event) and the spectra obtained excluding this event. In turn, this means that the fluence (F_P) is about one order of magni-

tude lower than that obtained from the upper-limit bound, for the corresponding F_{SXR}, when taking into account the 8 November 2000 event. However, when excluding this SEP event the obtained spectra for GLE05 underestimates the actual measured fluence at E>200 MeV & primarily at E>430 MeV, while for the AD774 SEP event the underestimation starts already at E>30 MeV (not shown), implying that the exclusion of this event underestimates the obtained fluence spectra at both cases. Scalings with F_{SXR} and $F_{SXR}^{7/6}$ were also applied and showed similar underestimates of the derived fluence in both cases. On top of these findings, to address the possible influence that the inclusion of the event on 8 November 2000 has in our calculations, we calculated the residuals of the relations I_P to F_{SXR} for each integral energy (see Figures 1 & 2) and showed that although there is a considerable spread for all 65 points, the residual of 8 November 2000 falls well within 3-S.D. (see details in Appendix B). Therefore, this event was not excluded from the analysis.

Differences in the obtained scaling laws of I_P distributions for flares alone and SEP associated flares are a general point of intensive research since Hudson (1978). According to Kahler & Ling (2020), there are three possibilities to account for such a discrepancy: (a) flares associated with SEPs are fundamentally different from ordinary flares; (b) flares associated with SEPs represent the high-end of the energy distribution of ordinary flares and (c) flares associated with SEPs exceed a threshold barrier. Cliver & D'Huys (2018) argues in favor of (a) and (c) indicating that this threshold is at a CME speed of ~400 km/s; above which a shock can be formed (see Figure 2 of Cliver & D'Huys 2018). This is further supported by the fact that fast CMEs are needed in order to drive shocks capable of accelerating SEPs. Moreover, this is also corroborated by Kahler & Ling (2020) who showed that flares associated with SEP events and/or fast

CMEs are characterized by lower flare temperatures than those without. On the other hand, (b) is favored by the work of Takahashi et al. (2016) although, Kahler (2013) argued against the validity of scaling laws in general. Nonetheless, scaling relations hold important information providing a representation of the expected conditions of the radiation environment.

An important point in the understanding of scaling laws is that such relations inherently assume that there is a flare, an associated CME and that there will always be a resulting SEP event. However, this one-to-one association scenario is not realistic, since from tens of thousands of recorded flares and CMEs we have only registered a few hundreds SEPs (Papaioannou et al. 2016). Therefore, scaling laws can offer context under the assumption that solar eruptive events will lead to the acceleration and escape of particles.

The theoretical arguments employed assume that a fraction (f) of the magnetic energy stored in an AR is released during a flare; the so-called flare energy (E_{flare}). In the literature, this fraction has been estimated to lie in the range 10 to 50% for large flares (Emslie et al. 2012; Schrijver et al. 2012). Understandably this fraction has a direct effect on the estimates of the solar/stellar radiation and particle environment (see discussion in Herbst et al. 2021).

Furthermore, another point to take into account stems from Reames & Ng (1998) who suggested that energetic particle intensities measured early in a SEP event are bounded by a maximum intensity plateau known as the "streaming limit". The mechanism at work is wave generation by particles streaming outward from an intense source near the Sun, and provides a self-regulation of the particle intensity (Ng & Reames 1994). As a result, energetic particles propagating along IMF lines reach a maximum intensity plateau because the scattering processes produced by self-generated waves restrict their streaming. Therefore, according to this scenario, particle intensities measured early in a large SEP event (known as the prompt component of the SEP event) are bounded by a certain upper limit. Scaling laws, in general, do not take into account the "streaming limit". However, they provide a simplified quantification of the relation between the driver (i.e. solar eruptive events) and the resulting SEP event, which is useful for the direct approximation of the expected I_P based on F_{SXR} and/or V_{CME}.

Extending the scaling relations we provide a direct estimation of the upper limit spectra based on F_{SXR}, alone considering all caveats and limitations described above. Such spectra is directly usable in the solar case. Admittedly, the form of the spectra deserves a more detailed investigation, nonetheless the power-law approximation employed in this work provides context since the observed spectral break energies in major SEPs are usually much greater than several ten's of MeV and usually fall above 200 MeV - especially for strong events (see Bruno et al. 2018).

In light of recent results showing that the Sun has been able to give rise to several extreme SEP events which are likely not manifestations of unknown phenomena but rather the high-energy/low-probability tail of the "regular" SEP distribution (Usoskin & Kovaltsov 2021), we have identified an *upper limit* to the spectrum of conditions produced by the extreme events (i.e. an upper limit ~X600 SXR flare (Cliver et al. 2020b) based on the AD774/775 cosmogenic nuclide event; Miyake et al. (2012)). We find that the F_P at E>200 MeV is ~ 10^{10} cm^{-2} and at E>430 MeV is ~1.5×10^9 cm^{-2}. In turn, this also means that the Sun produced several extreme solar flares in the past that most likely affected the Earth's radiation environment and evolution. It should further be noted that such extreme events in terms

of fluence could also be caused by two (see discussion on the AD774/775 SEP event in Cliver et al. 2020b) or three equal intensity SEP events (Cliver et al. 2022). To assess such a possibility, a re-scaled estimation of 3 x ~X140 SXR flares were used in this work and the obtained fluence for E>200 MeV and E>430 MeV were added in the inset of Figure 6, as red triangles to facilitate direct comparison.

The implications of our study extend to other Sun-like G-type stars that are known to produce superflares frequently (Maehara et al. 2012; Notsu et al. 2019; Okamoto et al. 2021). Unless the Sun is a unique star, one may assume that G-type stars show similar behavior. Thus our understanding of the Sun and its upper limits pertain to the efforts for assessing - within errors, caveats and limitations - their radiation environment and its impact on the habitability of potential exoplanets (see e.g. Youngblood et al. 2017; Herbst et al. 2019; Fraschetti et al. 2019; Herbst et al. 2021; Barth et al. 2021). In this regard, we further included the simulated/modelled cases of Hu et al. (2022) in our Figure 1 (not shown). Their modeled cases fall well within our sample and their obtained scaling for the simulated events are ~ two orders of magnitude lower than the fluxes estimated by Takahashi et al. (2016) and our work. As noted in Hu et al. (2022) the close similarity in the obtained scaling laws' power-law indices suggests that such laws derived from SEP events can be applied to stellar energetic particle events, as well. Although there are many more constrains to consider in the stellar case, our work is in agreement with such findings.

Takahashi et al. (2016) applied the concept of scaling laws to assess the upper limit of the Sun on space weather and the terrestrial environment. The current consensus is that the cosmogenic nuclide enhancements in the AD774 were the result of a SEP event (Miyake et al. 2019). While the detailed observations necessary to explain the outsized SEP event in AD774 are unavailable, it is desirable for worst-case space weather scenarios to make inferences about the circumstances under which it arose, viz., the values of both SXR flare peak intensity and CME speed. In this paper, we investigated the dependence of SEP events on F_{SXR} by applying a range of scaling laws starting with Takahashi et al. (2016) to the estimates of flare intensity for the AD774/775 event obtained by Cliver et al. (2020b, 2022). This study comprises the first of two investigations on the dependence of SEP events on their associated solar activities. In our subsequent work (i.e. *part II*), we will examine the dependence of SEP events on CMEs.

References

Agueda, N., Lario, D., Ontiveros, V., et al. 2012, Solar Physics, 281, 319
Airapetian, V. S., Barnes, R., Cohen, O., et al. 2020, International Journal of Astrobiology, 19, 136
Anastasiadis, A., Lario, D., Papaioannou, A., Kouloumvakos, A., & Vourlidas, A. 2019, Philosophical Transactions of the Royal Society A, 377, 20180100
Barth, P., Helling, C., Stüeken, E. E., et al. 2021, MNRAS, 502, 6201

Bazilevskaya, G., Makhmutov, V., Stozhkov, Y., Svirzhevskaya, A., & Svirzhevsky, N. 2010, Advances in space research, 45, 603

Belov, A., Bieber, J., Eroshenko, E., et al. 2001, in International Cosmic Ray Conference, Vol. 8, 3446

Belov, A., Eroshenko, E., Mavromichalaki, H., Plainaki, C., & Yanke, V. 2005, Advances in Space Research, 35, 697

Belov, A., Eroshenko, E., Mavromichalaki, H., Plainaki, C., & Yanke, V. 2005a, Annales Geophysicae, 23, 2281

Belov, A., Garcia, H., Kurt, V., Mavromichalaki, H., & Gerontidou, M. 2005b, Solar Physics, 229, 135

Belov, A., Kurt, V., Mavromichalaki, H., & Gerontidou, M. 2007, Sol. Phys., 246, 457

Belov, A. V. 2017, Geomagnetism and Aeronomy, 57, 727

Brehm, N., Christl, M., Adolphi, F., et al. 2021, Nature Geoscience, 14, 10

Bruno, A., Bazilevskaya, G. A., Boezio, M., et al. 2018, ApJ, 862, 97

Büntgen, U., Wacker, L., Galván, J. D., et al. 2018, Nature Communications, 9, 3605

Bütikofer, R., Kühl, P., & Papaioannou, A. 2021, in NMDB@ Home 2020: Proceedings of the 1st virtual symposium on cosmic ray studies with neutron detectors, 89–95

Cane, H. V., Erickson, W., & Prestage, N. 2002, Journal of Geophysical Research: Space Physics, 107, SSH

Cane, H. V., Richardson, I. G., & von Rosenvinge, T. T. 2010, Journal of Geophysical Research (Space Physics), 115, A08101

Chollet, E., Giacalone, J., & Mewaldt, R. 2010, Journal of Geophysical Research: Space Physics, 115

Chupp, E. L., Debrunner, H., Flueckiger, E., et al. 1987, ApJ, 318, 913

Cliver, E. 2016, The Astrophysical Journal, 832, 128

Cliver, E. W. & D'Huys, E. 2018, ApJ, 864, 48

Cliver, E. W. & Dietrich, W. F. 2013, Journal of Space Weather and Space Climate, 3, A31

Cliver, E. W., Hayakawa, H., Love, J. J., & Neidig, D. F. 2020b, ApJ, 903, 41

Cliver, E. W., Kahler, S. W., Kazachenko, M., & Shimojo, M. 2019, ApJ, 877, 11

Cliver, E. W., Ling, A. G., Belov, A., & Yashiro, S. 2012, ApJ, 756, L29

Cliver, E. W., Mekhaldi, F., & Muscheler, R. 2020a, The Astrophysical Journal Letters, 900, L11

Cliver, E. W., Schrijver, C. J., Shibata, K., & Usoskin, I. G. 2022, Living Reviews in Solar Physics, 19, 2

Desai, M. & Giacalone, J. 2016, Living Reviews in Solar Physics, 13, 1

Dierckxsens, M., Tziotziou, K., Dalla, S., et al. 2015, Sol. Phys., 290, 841

Emslie, A. G., Dennis, B. R., Shih, A. Y., et al. 2012, ApJ, 759, 71

Forrest, D., Vestrand, W., Chupp, E., et al. 1985, in 19th Intern. Cosmic Ray Conf-Vol. 4 No. SH-1.4-7

Fraschetti, F., Drake, J. J., Alvarado-Gómez, J. D., et al. 2019, ApJ, 874, 21

Harper, W. V. 2014, Wiley StatsRef: Statistics Reference Online, 1

Herbst, K., Papaioannou, A., Airapetian, V. S., & Atri, D. 2021, The Astrophysical Journal, 907, 89

Herbst, K., Papaioannou, A., Banjac, S., & Heber, B. 2019, A&A, 621, A67

Hu, J., Airapetian, V. S., Li, G., Zank, G., & Jin, M. 2022, Science Advances, 8, eabi9743

Hudson, H. S. 1978, Sol. Phys., 57, 237

Jiggens, P., Chavy-Macdonald, M.-A., Santin, G., et al. 2014, Journal of Space Weather and Space Climate, 4, A20

Kahler, S. W. 1982, J. Geophys. Res., 87, 3439

Kahler, S. W. 2001, J. Geophys. Res., 106, 20947

Kahler, S. W. 2013, ApJ, 769, 35

Kahler, S. W. & Ling, A. G. 2018, Solar Physics, 293, 1

Kahler, S. W. & Ling, A. G. 2020, ApJ, 901, 63

Kallenrode, M. & Cliver, E. 2001, in International Cosmic Ray Conference, Vol. 8, 3314

Kiplinger, A. L. & Garcia, H. A. 2004, in American Astronomical Society Meeting Abstracts, Vol. 204, American Astronomical Society Meeting Abstracts #204, 47.13

Klein, K.-L. & Dalla, S. 2017, Space Science Reviews, 212, 1107

Knipp, D. J., Fraser, B. J., Shea, M., & Smart, D. 2018, Space Weather, 16, 1635

Koldobskiy, S., Raukunen, O., Vainio, R., Kovaltsov, G. A., & Usoskin, I. 2021, Astronomy & Astrophysics, 647, A132

Kurt, V., Belov, A., Mavromichalaki, H., & Gerontidou, M. 2004, Annales Geophysicae, 22, 2255

Lammer, H., Selsis, F., Ribas, I., et al. 2003, ApJ, 598, L121

Lario, D. & Decker, R. B. 2011, Space Weather, 9, S11003

Lario, D., Ho, G. C., Roelof, E. C., Decker, R. B., & Anderson, B. J. 2013, in American Institute of Physics Conference Series, Vol. 1539, Solar Wind 13, ed. G. P. Zank, J. Borovsky, R. Bruno, J. Cirtain, S. Cranmer, H. Elliott, J. Giacalone, W. Gonzalez, G. Li, E. Marsch, E. Moebius, N. Pogorelov, J. Spann, & O. Verkhoglyadova, 215–218

Lario, D. & Karelitz, A. 2014, Journal of Geophysical Research (Space Physics), 119, 4185

Lario, D., Roelof, E., Decker, R., & Reisenfeld, D. 2003, Advances in Space Research, 32, 579

Maehara, H., Shibayama, T., Notsu, S., et al. 2012, Nature, 485, 478

Mavromichalaki, H., Papaioannou, A., Plainaki, C., et al. 2011, Advances in Space Research, 47, 2210

Mekhaldi, F., Muscheler, R., Adolphi, F., et al. 2015, Nature communications, 6, 1

Miroshnichenko, L. & Nymmik, R. 2014, Radiation measurements, 61, 6

Mishev, A. & Usoskin, I. 2016, Solar Physics, 291, 1225

Miyake, F., Nagaya, K., Masuda, K., & Nakamura, T. 2012, Nature, 486, 240

Miyake, F., Panyushkina, I. P., Jull, A. J. T., et al. 2021, Geophysical Research Letters, 48, e2021GL093419, e2021GL093419 2021GL093419

Miyake, F., Usoskin, I., & Poluianov, S. 2019, Extreme Solar Particle Storms; The hostile Sun

Ng, C. K. & Reames, D. V. 1994, ApJ, 424, 1032

Notsu, Y., Maehara, H., Honda, S., et al. 2019, ApJ, 876, 58

O'Hare, P., Mekhaldi, F., Adolphi, F., et al. 2019, Proceedings of the National Academy of Sciences, 116, 5961

Okamoto, S., Notsu, Y., Maehara, H., et al. 2021, The Astrophysical Journal, 906, 72

Paleari, C. I., Mekhaldi, F., Adolphi, F., et al. 2022, Nat Commun, 13

Papaioannou, A., Kouloumvakos, A., Mishev, A., et al. 2022, A&A, 660, L5

Papaioannou, A., Sandberg, I., Anastasiadis, A., et al. 2016, Journal of Space Weather and Space Climate, 6, A42

Poluianov, S. V., Usoskin, I. G., Mishev, A. L., Shea, M. A., & Smart, D. F. 2017, Sol. Phys., 292, 176

Raukunen, O., Vainio, R., Tylka, A. J., et al. 2018, Journal of Space Weather and Space Climate, 8, A04

Reames, D. V. 2021, Solar Energetic Particles. A Modern Primer on Understanding Sources, Acceleration and Propagation, Vol. 978

Reames, D. V. & Ng, C. K. 1998, ApJ, 504, 1002

Schaefer, B. E., King, J. R., & Deliyannis, C. P. 2000, The Astrophysical Journal, 529, 1026

Schrijver, C. J., Beer, J., Baltensperger, U., et al. 2012, Journal of Geophysical Research (Space Physics), 117, A08103

Shea, M. & Smart, D. 2012, Space science reviews, 171, 161

Shen, C., Wang, Y., Ye, P., & Wang, S. 2008, Sol. Phys., 252, 409

Smart, D., Shea, M., & McCracken, K. 2006, Advances in Space Research, 38, 215

Takahashi, T., Mizuno, Y., & Shibata, K. 2016, ApJ, 833, L8

Temmer, M. 2021, Living Reviews in Solar Physics, 18, 4

Thakur, N., Gopalswamy, N., Mäkelä, P., et al. 2016, Solar Physics, 291, 513

Till, R. 1973, Area, 303

Tschernitz, J., Veronig, A. M., Thalmann, J. K., Hinterreiter, J., & Pötzi, W. 2018, ApJ, 853, 41

Usoskin, I., Koldobskiy, S., Kovaltsov, G., et al. 2020, Astronomy & Astrophysics, 640, A17

Usoskin, I., Koldobskiy, S., Kovaltsov, G., et al. 2021, in Proceedings of 37th International Cosmic Ray Conference — PoS(ICRC2021), Vol. 395, 1319

Usoskin, I., Kromer, B., Ludlow, F., et al. 2013, Astronomy & Astrophysics, 552, L3

Usoskin, I. G., Koldobskiy, S. A., Kovaltsov, G. A., et al. 2020, Journal of Geophysical Research: Space Physics, 125, e2020JA027921, e2020JA027921 10.1029/2020JA027921

Usoskin, I. G. & Kovaltsov, G. A. 2021, Geophysical Research Letters, e2021GL094848

Usoskin, I. G., Kromer, B., Ludlow, F., et al. 2013, A&A, 552, L3

Vainio, R. 2003, Astronomy & Astrophysics, 406, 735

Youngblood, A., France, K., Loyd, R. O. P., et al. 2017, ApJ, 843, 31

Appendix A: The log(F_P) vs. log(I_p) relations

In our examination of the four integral energies employed, we find a very robust statistical linear correlation between logs of F_P and I_p over an energy range from E>10 MeV to E>100 MeV and over four decades of measurements (i.e., from 1984-2017) which is the period covered by the 65 SEP events of our sample. Figure A.1 presents the log-log relation of the F_P versus I_P for the four integral energy bands of the SEP events we considered. For all integral energies of interest, we performed linear RMA fits. Table A.1 summarizes the results. As it can be seen in Figure A.1 over nearly (or more than) four orders of magnitude a robust relation of the F_P vs I_P is found, as indicated by the high ($\sim$ 0.97) cc-values (see Table A.1). Thus, over an extensive range of event peak intensities I_P, these linear fits allow one to make estimates of the event fluences (F_P) from observed I_P within a factor of ≈ 1.65, in agreement with the findings of Kahler & Ling (2018).

F_P values are vital since they account for both the adiabatic energy losses and multiple traversals of particles across the observer position. The effect of both has been addressed by Chollet et al. (2010), who found that the two effects are generally equal and offsetting for a broad range of energies and over many ion species.

Table A.1. Slopes of F_P-I_P and plot amplitudes for each integral energy, derived in this work.

Integral Energy (MeV)	Slope F_P-I_P (δ)	Plot amplitude	Correlation Coefficient (cc)
E>10	1.13±0.04	5.48±0.07	0.96
E>30	1.13±0.04	5.46±0.06	0.97
E>60	1.08±0.03	5.51±0.06	0.97
E>100	1.02±0.03	5.53±0.06	0.97

Table A.2. Comparison of fluence values for E>100 MeV derived in this work and in CL16.

E>100 MeV Fluence [$\cdot$ 10^3 cm^{-2} sr^{-1}]		
Date	this work	CL16
02/04/2001	241	220
08/11/2000	13300	13000
17/05/2012	338	305
24/08/2002	434	400
20/01/2005	6470	6400
13/12/2006	1880	1900
21/04/2002	1530	1500
26/01/2001	637	630

While evaluating the obtained values for the fluence, we surveyed the literature to identify previously published fluences at the respective energies. Cliver (2016, hereafter CL16) lists the fluence at E>100 MeV (in protons (cm^{-2} sr^{-1})) for a set of intense SEP events (see their Table 1) while Koldobskiy et al. (2021, hereafter KL21) tabulates the fluence (in protons (cm^{-2}) for all integral energies of interest in this study (i.e. E>10-; >30-; >60-; and >100 MeV) for 26 GLEs recorded from 1989 - 2017 (see their Table 1). Out of these, 16 GLEs were also present in our catalog employed in this study. The comparisons are given in the following Tables A.2 and A.3. As can be seen, the comparison of the derived fluences shows an excellent agreement between the calculations of this study and the outputs of CL16 (see

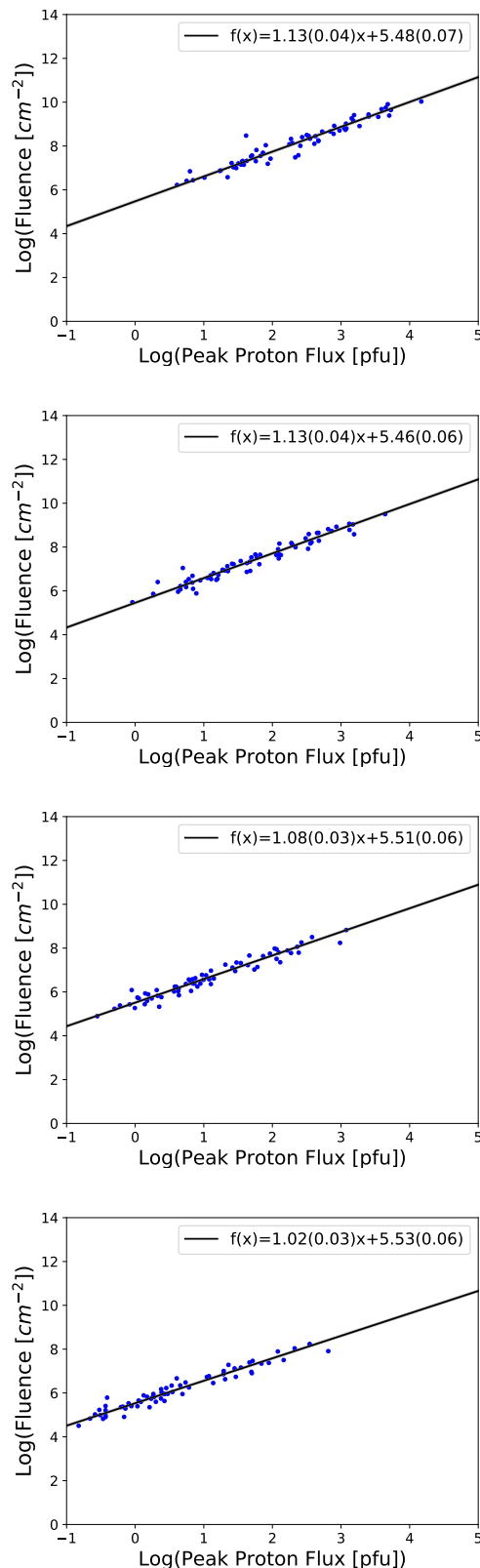**Fig. A.1.** Log F_P versus log I_P for the four integral energy bands of the SEP events, i.e. (from top to bottom) E>10-; E>30-; E>60-; and E>100 MeV, respectively. In all cases the black solid line presents the RMA regression line.

Table A.2) and Figure A.3. The results agree within a mean factor of ~ 1.04. At the same time, the comparison between the ob-

tained omnidirectional fluences in this work and those presented in KL21 show a less strong but still reasonable agreement for E>10 MeV (a mean factor of ~ 2.20). However, when shifting to higher energy (i.e. E>100 MeV) the agreement gets stronger (a mean factor of ~ 1.02, see Table A.3 and Figure A.4). In both comparisons, a close relationship between the obtained fluences at each energy obtained in this work and CL16 and KL21 is evident by the high cc (≥0.98). However, one should note that as highlighted in Section 2, different *GOES* spacecraft lead to differences between the intensities. As a result, this affects the derived peak proton flux and consequently the calculated fluence at each case. For example, out of the 16 GLEs, KL21 and this study used measurements from the same *GOES* spacecraft for only seven events (~43% of the cases). If the comparison considers only these seven events, the mean factor for E>10 MeV falls to ~1.30. Figure A.2, is similar to Figure 6. It presents the fluence range from the 65 SEP events with a gray shaded area and the mean (median) spectrum obtained from the measurements as blue(magenta) lines. The blue bars denote the range of the fluence at the respective integral energies from Table A.3. As a result, the obtained fluence values for the GLEs seem to lie within the gray shaded area.

Fig. A.2. A plot similar to Figure 6. Here the range from the 65 SEP events is presented with a gray shaded area, the magenta line provides the mean and the blue line the median spectrum from the measurements. The blue bars denote the range of the fluence at the respective integral energies from Table A.3.

Table A.3. Comparison of fluence values for E>10-; E>30-; E>60; and E>100 MeV derived in this work and in KL21.

Fluence [cm^{-2}]			
	E>10 MeV		**E>30 MeV**
Event	**this work**	**KL21**	**this work**	**KL21**
GLE40	1.60E+07	9.18E+06	7.97E+06	6.84E+06
GLE41	1.82E+09	5.02E+08	3.90E+08	1.67E+08
GLE44	4.36E+09	1.62E+09	1.16E+09	8.20E+08
GLE45	2.21E+09	7.94E+08	5.43E+08	3.68E+08
GLE46	1.40E+07	5.54E+06	5.45E+06	4.33E+06
GLE47	1.27E+08	4.78E+07	4.35E+07	2.71E+07
GLE48	1.21E+08	3.18E+07	4.60E+07	2.35E+07
GLE52	2.54E+08	6.81E+07	4.46E+07	2.17E+07
GLE55	4.56E+08	3.17E+08	1.54E+08	1.25E+08
GLE60	5.12E+08	4.51E+08	1.45E+08	1.35E+08
GLE63	3.58E+08	3.13E+08	8.34E+07	7.91E+07
GLE64	3.18E+08	2.27E+08	4.87E+07	4.31E+07
GLE67	1.43E+09	5.73E+08	1.95E+08	1.37E+08
GLE69	8.13E+08	6.98E+08	3.84E+08	3.57E+08
GLE70	4.62E+08	3.55E+08	1.67E+08	1.55E+08
GLE71	1.02E+08	6.85E+07	3.03E+07	2.44E+07
	E>60 MeV		**E>100 MeV**
Event	**this work**	**KL21**	**this work**	**KL21**
GLE40	3.75E+06	4.40E+06	1.78E+06	1.97E+06
GLE41	8.91E+07	6.39E+07	2.93E+07	2.27E+07
GLE44	3.17E+08	3.74E+08	1.09E+08	1.15E+08
GLE45	1.81E+08	2.07E+08	7.85E+07	8.39E+07
GLE46	2.41E+06	3.55E+06	1.10E+06	1.53E+06
GLE47	1.67E+07	1.74E+07	7.24E+06	7.28E+06
GLE48	2.08E+07	1.85E+07	1.01E+07	9.08E+06
GLE52	8.93E+06	8.85E+06	2.86E+06	2.77E+06
GLE55	5.59E+07	4.97E+07	2.46E+07	2.27E+07
GLE60	6.19E+07	5.83E+07	3.19E+07	3.02E+07
GLE63	2.26E+07	2.18E+07	8.00E+06	7.74E+06
GLE64	1.37E+07	1.27E+07	5.45E+06	5.06E+06
GLE67	3.23E+07	2.80E+07	9.18E+06	9.19E+06
GLE69	1.73E+08	1.66E+08	8.13E+07	7.85E+07
GLE70	5.96E+07	5.70E+07	2.36E+07	2.27E+07
GLE71	1.05E+07	9.21E+06	4.25E+06	3.93E+06

As a next step, the annual fluence *versus* the annual peak proton flux for each integral energy of interest was investigated. As stated before, we find a very robust statistical linear correlation between logs of F_P and I_p for each integral energy. Therefore, the linear relations seem to be evident in the annual case, as well. Figure A.5 presents the log-log relation of the F_P versus I_P for the four integral energy bands. For all integral energies of interest, we performed linear RMA fits. As it can be seen in Figure A.5 over nearly (or more than) four orders of magnitude a robust relation of the F_P vs I_P is found. Again, in the annual case high (~ 0.97) *cc*-values are obtained (see Table A.4).
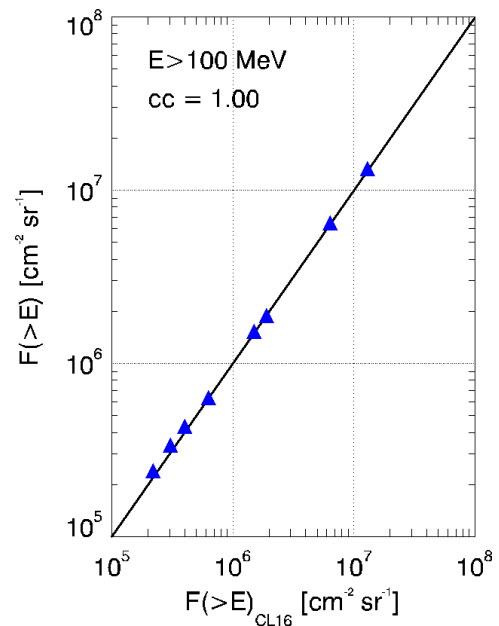
Fig. A.3. Scatter plot of the integral fluences F(>E) obtained from the data in this work (Y-axis) and from the work of Cliver (2016) (CL16; X-axis) for E>100 MeV. Blue triangles correspond to individual SEP events (see Table A.2), and the solid black line denotes the diagonal dichotomous.
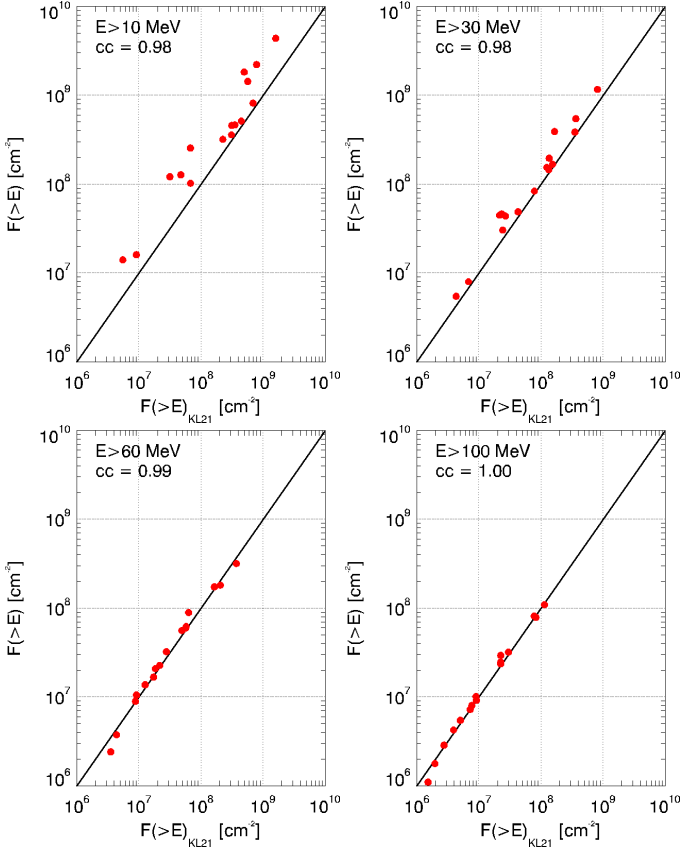
Fig. A.4. Similar to Figure A.3. Scatter plots of the integral fluences F(>E) obtained from the data in this work (Y-axis) and from the work of Koldobskiy et al. (2021) (KL21; X-axis) for each integral energy of interest. Red circles correspond to individual GLE events (see Table A.3), and the solid black line denotes the diagonal dichotomous of each panel.

Fig. A.5. A plot similar to Figure A.1 but for annual values. Each integral energy is presented with a different color (i.e. E>10 MeV - blue; E>30 MeV - red; E>60 MeV - green and E>100 MeV - orange). The obtained linear fit is depicted as a solid line in each panel, while the dotted lines demonstrate the 1-σ error of the fit. The corresponding correlation coefficients ($cc's$) are further presented on each plot.

Table A.4. Slopes of F_P-I_P and plot amplitudes for each integral energy for the annual case, derived in this work.

Integral Energy (MeV)	Slope F_P-I_P (annual)	Plot amplitude	Correlation Coefficient (cc)
E>10	1.09±0.04	5.62±0.18	0.96
E>30	1.07±0.04	5.61±0.12	0.98
E>60	1.02±0.03	5.59±0.05	0.99
E>100	0.98±0.04	5.56±0.05	0.99

Appendix B: The 8 November 2000 event

As indicated in the manuscript the 8 November 2000 event is the one event that is clearly distinguished as the one with the largest obtained peak proton flux for a relatively modest SXR flare. We assess the departure of this particular event from the linear fit obtained in Figures 1 & 2 by calculating the residuals as: *residual = predicted y − actual y*, and the standard deviation of the residuals (i.e. S.D.). Figure B.1 demonstrates these calculated residuals for each integral energy of interest (i.e. E>10; E> 30; E>60 and E>100 MeV) as black circles. The residuals lie on the vertical axis, while the SXR magnitude (i.e. the independent variable) is on the horizontal axis. The dotted blue line represents the perfect agreement of the fitted value to the actual one. The *S.D.* for each integral energy is presented on each panel of Figure B.1. It ranges from S.D.=0.68 (E>10 MeV) to S.D.=0.62 (E>100 MeV). The 8 November 2000 event is indicated with a red circle. As it can be seen, there is a random dispersion of all points around the perfect fit (i.e. the blue dotted line). Moreover, all points seem to have a large spread with the minimum and maximum residual printed in the legend of each panel of Figure B.1. Finally, the residuals of 8 November 2000 event lie well within 3-S.D. in each integral energy of interest.
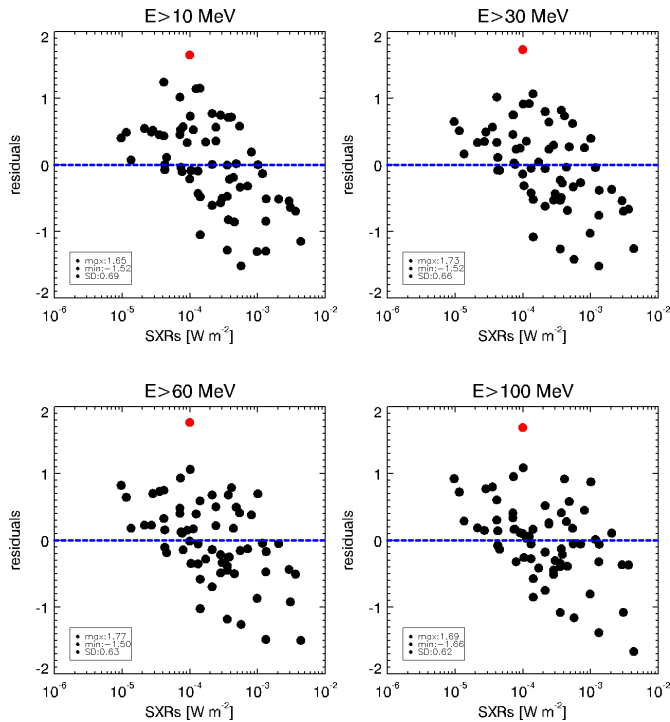
Fig. B.1. The calculated residuals *versus* the SXR flux for all 65 events of our sample. Each panel corresponds to an integral energy (E>10-; E>30-; E>60-; E>100 MeV). In each panel the red point depicts the 8 November 2000 event. The legend provides the standard deviation (S.D.) of the residuals, as well as, the min and the max residual of the sample.

Appendix C: The complete list of SEP events utilized in this study

Here we provide a listing of the SEP events, their achieved peak proton flux and fluence at each integral energy of interest as well as their parent solar events.

Proton Event — Fluence [/cm²] and Peak Proton Flux [pfu]; Solar Flare Event; Coronal Mass Ejection (CME)

No	Year	Date	Time (UT)	Fluence >10 MeV	Fluence >30 MeV	Fluence >60 MeV	Fluence >100 MeV	Peak >10 MeV	Peak >30 MeV	Peak >60 MeV	Peak >100 MeV	GOES sat.	Flare Date	Flare Time (UT)	Lon	Lat	X-ray Peak	CME Width (deg)	CME Speed (Km/s)
1	1984	14-Mar	4:05	3.14E+07	8.05E+06	3.09E+06	1.41E+06	66.61	14.95	7.19	3.01		14-Mar	3:15	42	-12	M2		
2	1985	22-Jan	1:20	7.01E+06	2.54E+06	1.22E+06	6.13E+05	6.28	2.13	0.89	0.39		21-Jan	23:52	38	-8	X4		
3	1985	9-Jul	2:25	1.54E+07	3.19E+06	1.05E+06	4.50E+05	85.68	15.21	3.69	1.12		9-Jul	1:26	27	-13	M2.9		
4	1986	7-Feb	13:00	1.36E+08	2.16E+07	3.58E+06	8.90E+05	196	47.1	9.89	2.68		7-Feb	10:11	20	-10	M5		
5	1986	10-Feb	21:00	2.57E+06	6.39E+05	1.71E+05	6.77E+04	5.62	1.86	0.5	0.22	5	10-Feb	20:25	32	-1	C9.5		
6	1986	14-Feb	10:35	2.10E+08	2.32E+07	3.39E+06	9.03E+05	187	34.5	6.22	1.84	5	14-Feb	9:10	76	1	M6.4		
7	1988	12-Oct	3:40	2.75E+06	7.33E+05	2.41E+05	1.05E+05	6.97	1.83	0.6	0.26	7	12-Oct	4:57	66	-20	X2.5		
8	1989	23-Mar	20:30	9.82E+06	1.24E+06	2.74E+05	7.98E+04	29.7	6.97	1.38	0.37	7	23-Mar	19:25	28	18	X1.5		
9	1989	18-Jun	15:00	3.60E+06	1.50E+06	5.82E+05	2.47E+05	10.2	5.52	2.41	1.08	7	18-Jun	16:19	57	15	C6.8		
10	1989	25-Jul	9:05	1.60E+07	7.96E+06	3.75E+06	1.78E+06	32	22.5	12	6.08	7	25-Jul	8:39	84	25	X2.6		
11	1989	12-Aug	15:30	5.64E+09	1.08E+09	1.14E+08	1.44E+07	4490	1490	230	34.8	7	12-Aug	13:57	37	-16	X2.6		
12	1989	16-Aug	1:30	1.82E+09	3.90E+08	8.90E+07	2.93E+07	1430	339	115	51.5	7	16-Aug	1:08	84	-18	X20		
13	1989	22-Oct	16:30	4.36E+09	1.16E+09	3.17E+08	1.09E+08	5330	1320	378	211	7	22-Oct	17:08	31	-27	X2.9		
14	1989	24-Oct	19:00	2.21E+09	5.43E+08	1.81E+08	7.85E+07	2530	729	265	120	7	24-Oct	17:36	57	-30	X5.7		
15	1989	15-Nov	7:05	1.40E+07	5.44E+06	2.41E+06	1.10E+06	38.3	16.3	7.28	3.49	7	15-Nov	6:38	26	11	X3.2		
16	1989	30-Nov	13:15	2.14E+09	1.29E+08	6.05E+06	3.94E+05	3490	195	9.42	1.21	7	30-Nov	11:45	52	24	X2		
17	1990	21-May	22:25	1.27E+08	4.35E+07	1.67E+07	7.24E+06	409	114	43.9	19.3	7	21-May	22:12	36	35	X5		
18	1990	24-May	20:35	1.21E+08	4.60E+07	2.08E+07	1.01E+07	177	56.4	34.6	19.5	7	24-May	20:46	78	33	X9.3		
19	1991	15-Jun	8:50	1.05E+09	2.50E+08	6.30E+07	2.20E+07	1180	305	124	69.3	7	15-Jun	6:33	69	33	X12		
20	1991	30-Oct	6:55	2.65E+07	9.22E+06	3.70E+06	1.68E+06	94	18.8	6.05	2.84	7	30-Oct	6:11	25	-8	X2.5		
21	1992	25-Jun	20:15	2.54E+08	4.48E+07	8.92E+06	2.86E+06	271	66.2	28.7	13.7	7	25-Jun	19:47	67	9	X3.9		
22	1992	30-Oct	18:25	2.56E+09	4.48E+08	4.33E+07	5.38E+06	1550	468	73.1	11.1	7	30-Oct	17:02	61	-22	X1.7		
23	1993	4-Mar	12:40	7.30E+06	1.66E+06	5.03E+05	1.94E+05	17.1	4.56	1.74	0.72	7	4-Mar	12:17	56	-14	C8.1		
24	1993	12-Mar	18:30	2.08E+07	3.91E+06	1.08E+06	3.96E+05	36.8	11.3	4.23	2	7	12-Mar	16:48	51	0	M7		
25	1994	19-Oct	21:45	1.41E+07	1.17E+06	2.70E+05	9.69E+04	34.9	4.56	0.83	0.31	7	19-Oct	22:35	24	12	M3.2		
26	1997	4-Nov	6:05	3.54E+07	8.49E+06	2.44E+06	9.43E+05	67.1	20.3	6.93	2.55	8	4-Nov	5:52	33	-14	X2.1		785
27	1997	6-Nov	12:20	4.56E+08	1.54E+08	5.59E+07	2.46E+07	532	189	92	46.3	8	6-Nov	11:49	63	-18	X9.4		1556
28	1998	6-May	8:15	3.79E+07	8.18E+06	2.28E+06	8.97E+05	239	47.5	12.7	4.89	8	6-May	7:58	65	-11	X2.7	248	1099
29	1998	30-Sep	14:10	5.48E+08	4.33E+07	4.09E+06	9.12E+05	1160	133	14	2.98	8	30-Sep	13:04	85	19	M2.9	……	1108
30	2000	10-Jun	17:00	2.09E+07	3.47E+06	7.07E+05	2.23E+05	42.2	12.8	4.34	1.62	8	10-Jun	16:40	38	22	M5.2	259	1230
31	2000	22-Jul	11:50	7.66E+06	9.17E+05	1.85E+05	6.59E+04	17.6	4.22	0.99	0.34	8	22-Jul	11:17	56	14	M3	170	1738
32	2000	8-Nov	23:20	1.07E+10	3.18E+09	6.67E+08	1.73E+08	14800	4400	1190	349	8	8-Nov	22:42	77	10	M7	360	916
33	2001	28-Jan	16:45	3.36E+07	3.45E+06	5.56E+05	1.69E+05	48.9	6.03	1.08	0.3	8	28-Jan	15:40	59	-4	M1.5	80	992
34	2001	2-Apr	11:20	1.66E+06	1.66E+05	3.19E+04	3.19E+04	4.07	0.91	0.28	0.15	8	2-Apr	10:58	62	17	X1		
35	2001	2-Apr	23:15	6.61E+08	9.79E+07	1.29E+07	3.02E+06	1110	217	26.2	5.42	8	2-Apr	21:32	82	14	X20	244	2505
36	2001	12-Apr	11:20	3.71E+07	6.54E+06	1.74E+06	6.69E+05	50.5	13.9	3.95	1.49	8	12-Apr	9:39	43	-19	X2	360	1184
37	2001	15-Apr	13:50	5.12E+08	1.45E+08	6.19E+07	1.45E+07	951	357	242	146	8	15-Apr	13:19	85	-20	X14.4	167	1199
38	2001	23-Nov	1:05	8.08E+09	8.47E+08	4.57E+07	4.65E+06	4800	857	46.1	4.03	8	23-Nov	22:38	36	-17	M9.9	360	1437
39	2001	26-Dec	5:45	3.58E+08	8.33E+07	2.26E+07	8.00E+06	780	331	130	50.2	8	26-Dec	4:32	54	8	M7.1	212	1446
40	2002	21-Apr	1:40	2.73E+08	6.59E+07	1.92E+07	9.56E+06	2520	649	108	22.9	8	21-Apr	0:43	84	-14	X1.5	360	2393
41	2002	22-Aug	2:25	1.97E+07	5.12E+06	1.45E+06	5.47E+05	36.4	12.6	4.3	1.71	8	22-Aug	1:47	62	-7	M5.4	360	998
42	2002	24-Aug	1:15	3.17E+07	1.84E+07	1.37E+07	5.45E+06	317	123	60.4	29.3	8	24-Aug	0:49	81	-2	X3.1	360	1913
43	2003	31-May	2:40	1.09E+07	1.84E+06	6.69E+05	2.51E+05	27	6.79	2.12	0.88	8	31-May	2:13	65	-7	M9.3	360	1835
44	2003	26-Oct	17:40	1.81E+08	1.95E+07	1.75E+06	3.38E+05	466	42.6	3.78	0.8	11	26-Oct	17:21	38	2	X1.2	360	1537
45	2003	2-Nov	17:20	1.43E+09	2.92E+08	3.22E+07	9.18E+06	1510	476	115	49.4	11	2-Nov	17:03	56	-14	X8.3	360	2598
46	2003	4-Nov	21:40	2.14E+08	3.26E+07	3.80E+06	7.76E+05	353	59.3	6.85	1.33	11	4-Nov	19:29	83	-19	X28	360	2657
47	2004	19-Sep	17:25	2.03E+07	3.02E+06	3.91E+05	9.35E+04	57.3	8.87	1.49	0.37	11	19-Sep	16:46	58	3	M1.9	……	……
48	2004	10-Nov	3:05	2.81E+08	3.38E+07	4.24E+06	1.07E+06	424	49.4	7.52	2.42	11	10-Nov	1:59	49	9	X2.5	360	3387
49	2005	17-Jan	12:25	2.44E+09	6.04E+08	7.84E+07	1.32E+07	5040	1330	166	28.1	11	17-Jan	6:59	25	15	X3.8	360	2547
50	2005	20-Jan	6:40	8.13E+08	3.83E+08	1.73E+08	8.13E+07	1860	1550	968	652	11	20-Jan	6:36	61	14	X7.1	360	3256
51	2005	22-Aug	19:10	2.92E+08	1.65E+07	1.22E+06	2.56E+05	337	27.2	2.06	0.37	11	22-Aug	16:46	65	-13	M5.6	360	2378
52	2006	13-Dec	2:35	4.62E+08	1.67E+08	5.96E+07	2.36E+07	698	372	187	88.7	11	13-Dec	2:14	23	-6	X3.4	360	1774
53	2006	14-Dec	22:40	3.03E+07	7.32E+06	1.76E+06	5.57E+05	215	42.3	8.07	2.38	11	14-Dec	21:07	46	-6	X1.5	360	1582
54	2011	7-Jun	6:55	4.93E+07	1.73E+07	5.74E+06	2.22E+06	72.87	25.84	10.81	4.53	13	7-Jun	6:16	54	-21	M2.5	360	1042
55	2011	4-Aug	4:05	1.09E+08	3.56E+07	2.30E+07	6.56E+05	80.05	22.04	5.48	1.8	13	4-Aug	3:41	36	19	M9.3	360	1255
56	2011	9-Aug	8:10	1.11E+07	3.56E+06	1.11E+06	4.34E+05	26.92	15.83	6.52	2.67	13	9-Aug	7:48	69	17	X6.9	360	338
57	2012	23-Jan	4:10	4.81E+09	4.41E+08	1.76E+07	1.50E+06	3895.4	447.84	20.63	2.39	13	23-Jan	3:38	25	18	M8.7	360	2175
58	2012	27-Jan	17:55	8.33E+08	1.43E+08	2.20E+07	5.85E+06	795.5	126.43	29.96	11.88	13	27-Jan	17:37	71	27	X1.7	360	2508
59	2012	13-Mar	17:35	1.68E+08	1.64E+07	2.40E+06	6.66E+05	468.77	64.49	8.91	1.89	13	13-Mar	17:12	59	19	M7.9	360	1884
60	2012	17-May	1:30	1.02E+08	5.05E+07	1.05E+07	4.24E+06	255.44	123.65	54.54	20.44	13	17-May	1:25	76	11	M5.1	360	1582
61	2012	6-Jul	23:55	1.67E+07	2.56E+06	5.05E+05	1.63E+05	25.4	5.49	1.13	0.37	13	6-Jul	23:01	51	-17	X1	360	1828
62	2013	22-May	14:20	6.35E+08	7.97E+07	9.34E+06	2.18E+06	1196.6	121.05	12.73	3.4	15	22-May	13:08	70	15	M5.0	360	1466
63	2014	20-Feb	8:15	3.78E+06	7.70E+05	2.10E+05	8.10E+04	22.25	7.79	2.24	0.69	13	20-Feb	7:26	73	15	M3.0	360	948
64	2014	18-Apr	13:40	6.58E+07	4.86E+06	7.77E+05	2.37E+05	58.47	6.85	1.55	0.66	13	18-Apr	12:31	34	-2	M7.3	360	1203
65	2017	6-Sep	12:35	2.98E+07	1.11E+07	8.59E+05	2.28E+05	41.38	4.95	1.4	0.62	13	06-Sep	11:53	33	-8	X9.3	360	15711